EFFECT OF Ca^{2+} ON CO_2 CORROSION OF CARBON STEEL

By

MUHAMAD RIDZUAN BIN SHAEDIN (ID: 10210)

Dissertation

Submitted to the Petroleum Engineering Programme
in partial fulfillment of the requirements
for the Degree
Bachelor of Engineering (Hons) in
Petroleum Engineering

UNIVERSITI TEKNOLOGI PETRONAS
Bandar Seri Iskandar
31750 Tronoh
Perak Darul Ridzuan.

April 2011

STATUS OF DISSERTATION

EFFECT OF Ca^{2+} ON CO_2 CORROSION OF CARBON STEEL

I **MUHAMAD RIDZUAN BIN SHAEDIN** hereby allow my thesis to be placed at the Information Resource Center (IRC) of Universiti Teknologi PETRONAS with the following conditions:

1. The thesis becomes the property of Universiti Teknologi PETRONAS
2. The IRC of Universiti Teknologi PETRONAS may make copies of the thesis for academic purposes only.
3. This thesis is classified as

	Confidential
/	Non-confidential

Endorsed by:

Muhamad Ridzuan Bin Shaedin
Date: 8 April 2011

Assoc Prof Ir. Abdul Aziz Bin Omar
Project Supervisor
Date: 13-5-11

CERTIFICATION OF APPROVAL

EFFECT OF Ca^{2+} ON CO_2 CORROSION OF CARBON STEEL

By

Muhamad Ridzuan Bin Shaedin

A project dissertation submitted to the
Petroleum Engineering Programme
Universiti Teknologi PETRONAS
in partial fulfillment of the requirement for the
Bachelor of Engineering (Hons) in
Petroleum Engineering

Approved by:

Assoc Prof Ir. Abdul Aziz Bin Omar
Project Supervisor
Date: 13-5-11

UNIVERSITI TEKNOLOGI PETRONAS
Bandar Seri Iskandar
31750 Tronoh
Perak Darul Ridzuan.

April 2011

CERTIFICATION OF ORIGINALITY

This is to certify that I am responsible for the work submitted in this project, that the original work is my own except as specified in the references and acknowledgements, and that the original work contained herein have not been undertaken or done by unspecified sources or persons.

Muhamad Ridzuan Bin Shaedin

Date: 8 April 2011

ACKNOWLEDGEMENT

I would like to express my sincere gratitude and deep appreciation to the following people for their support, patience and guidance. Without them, this research wouldn't have been made possible. It is to them that I owe my gratitude.

- ***Assoc Prof Ir. Abdul Aziz Bin Omar*** for his expert guidance, continuous encouragement and patience. He has provided immense supervision and steered me in the proper direction. Among all the people whom I have/will come across in life, he will always stand out for his kindness, support, and understanding.

- ***Mr. Martin Choirul Fatah and Dr. Yuli Panca Asmara*** for their assistance, encouragement, guidance and excellent advice throughout this research project. Their continuous support and constant patience have taught me about discipline and ownership in completing this project.
- ***Assoc Prof Ir. Dr Mokhtar Bin Che Ismail*** for allowing me to use the corrosion laboratory facilities for my research.

Finally, above all, I would also like to thank my family, friends, and UTP lecturers for their unwavering love, support and assistance throughout the project.

ABSTRACT

In the sweet oil and gas fields, the formation water contained many cations such as Ca^{2+}, which lead to precipitation of scales and may influence the susceptibility to uniform and localized corrosion during CO_2 corrosion. Previous research related to effect of Ca^{2+} concentration in localized corrosion, less research focused on general CO_2 corrosion of carbon steel. The present study aimed at filling this gap by performing general CO_2 corrosion study in the solution of rich Ca^{2+}. Linear polarization resistance (LPR) technique was used to investigate the effect of Ca^{2+} concentration on general CO_2 corrosion of carbon steel X-52 under static condition. Ca^{2+} was added to the solution of NaCl as $CaCl_2$ to simulate the formation water. Ca^{2+} concentration in the simulated solution was set up at 0, 7000, 10000 and 20000 ppm. The experiments were carried out at constant Cl^- concentration of 36397.54 ppm to eliminate the effect of Cl^- on CO_2 corrosion of carbon steel. The temperature was set at 50°C and 80°C to simulate the real field condition. The results show that at the same Cl^- concentration, the corrosion rate decreases with present of Ca^{2+} in the solution and increases with increasing Ca^{2+} concentration from 7000 ppm to 20000 ppm. $CaCO_3$ scale forms a protective layer on the metal surface, hence reduce the corrosion rate. However, increase in Ca^{2+} will cause the corrosion scales become looser, which will cause the protectiveness of scales decrease. The corrosion rate increase with increasing temperature from 50°C to 80°C. This is due to the acceleration of anodic and cathodic reactions when temperature increases.

TABLE OF CON TENTS

LIST OF FIGURES

LIST OF TABLES

LIST OF ABBREVIATIONS

CO_2	Carbon dioxide
Cr	Chromium
LPR	Linear Polarization Resistance
SEM	Scanning Electron Microscopy
Ca^{2+}	*Calcium ion*
XRD	X-ray Diffraction
E_{corr}	Corrosion potential
I_{corr}	Current density

CHAPTER 1
INTRODUCTION

1.1 Background of Study

The CO_2 corrosion called "sweet corrosion" has been one of the important problems in oil and gas industry because of a high corrosion rate. Corrosion due to CO_2 is governed by a complex mixture of various mechanisms. A large number of parameters are involved and they affect the corrosion mechanism differently. The severity of corrosion depends particularly on temperature, CO_2 partial pressure, pH and material characteristics.

In the sweet oil and gas fields, the formation water contained many other cations such as Ca^{2+}, Mg^{2+} and so on, which lead to precipitation of scale deposits and may influence the corrosion behaviour of carbon steels. Although many studies in the laboratory and have been carried out to simulate CO_2 corrosion behaviour of carbon steel in NaCl solutions, less work has focused on corrosion problems of carbon steel in NaCl solution in the presence of Ca^{2+}. Therefore, it was decided to add different concentrations of Ca^{2+} (in the form of $CaCl_2$) into NaCl solution in the laboratory to simulate the aqueous medium from the real field in order to improve the understanding of carbon steels corrosion in the presence of Ca^{2+}.

In this project, the effect of Ca^{2+} concentration on general CO_2 corrosion of carbon steel was studied by electrochemical measurement of Linear Polarization Resistance (LPR) under static condition. It is expected that this research with provide an essential insight into the corrosion of carbon steel with high concentration of Ca^{2+} in a CO_2 environment.

1.2 Problem Statement

CO_2 corrosion has been of interest to researchers in oil and gas industries for many years and there exists many theories about the mechanisms of CO_2 corrosion. The mechanisms of CO_2 corrosion is not fully understood due to the complex reaction mechanisms and the presence of multiple factors including temperature, pressure, pH, composition of aqueous stream, partial pressures of CO_2, presence of non-aqueous phases, flow conditions and metal characteristics. In oil and gas industry, carbon steel represents the most commonly used material for well tubular, pipelines and other components. Unfortunately, carbon steel has low resistance to CO_2 corrosion. Therefore, the understanding on the limitations of the use of carbon steel will result a huge potential of economic savings. In oil and gas fields, mineral ion such as Ca^{2+} is naturally present in formation water. This mineral ion can precipitate and form scales which my influence the corrosion behaviour in a CO_2environment. Most of the previous research related to the effect of Ca^{2+} on CO_2 corrosion focused on the effect of Ca^{2+} concentration in localized corrosion. Less research focused on general CO_2 corrosion of carbon steel in the solution containing Ca^{2+}. The present study aimed at filling this gap by performing general CO_2 corrosion experiments in the solution of rich Ca^{2+}.

1.3 Objectives

1. To study the effect of Ca^{2+} on general CO_2 corrosion of carbon steel.
2. To study the effect of temperature on CO_2 corrosion rate in the solution containing Ca^{2+}.

1.4 Scope of Study

This study evolved around the effect of Ca^{2+} on general CO_2 corrosion of carbon steel. Electrochemical measurement of Linear Polarization Resistance (LPR) was used to measure the corrosion rate of carbon steel. Ca^{2+} was added to the solution of NaCl as $CaCl_2$ to simulate the formation water. Ca^{2+} concentration in the simulated solution was set up at 0, 7000, 10000 and 20000 ppm. The experiments were carried out at constant Cl^- concentration of 36397.54 ppm to eliminate the effect of Cl^- on CO_2 corrosion of carbon

steel. The effect of temperature on CO_2 corrosion rate was studied by setting up the temperature at 50°C and 80°C to simulate the real field condition.

1.5 Project Relevancy

1. Carbon steel for well tubular, pipelines and other components in oil and gas industry has advantages in terms of availability, cost and ease of fabrication over other alloys. Unfortunately, carbon steel has lower resistance to CO_2 corrosion. Thus, the understanding on the limitations of the use of carbon steel will result a huge potential of economic savings.
2. Even though there are many extensive CO_2 corrosion studies, less works focus on CO_2 corrosion in the solution of rich Ca^{2+}. As the result, the mechanism of CO_2 corrosion in the present of Ca^{2+} is still not clear. This lack of understanding has cause many failures in the field. For example, severe CO_2 corrosion of tubing was reported in the Shengli Oil field in the present of 15g/L Ca^{2+} [17].
3. The selection of corrosion control of carbon steel components in oil and gas production by the use of corrosion inhibitor and corrosion allowance take into account various parameter that govern the CO_2 corrosion such the present of Ca^{2+} in formation water. This research will provide an essential insight of the effect of Ca^{2+} on CO_2 corrosion which later helps to design an appropriate corrosion control method.

1.6 Feasibility of the Project

This research was feasible to be conducted within the given time frame due to following factors:

1. **Availability of equipments**
   Electrochemical measurement of Linear Polarization Resistance (LPR) is available at Academic Building 17, Universiti Teknologi PETRONAS.
2. **Availability of materials and chemicals**
   The required chemicals and materials for experimental works are provided at UTP laboratory facilities.

CHAPTER 2

LITERATURE REVIEW

2.1 CO_2 corrosion mechanisms

CO_2 corrosion is an electrochemical process which involves anodic dissolution of iron and cathodic evolution of hydrogen (Chilingar et al., 2008 and Callister, 2007) [13, 25]. Several mechanisms have been proposed on CO_2 corrosion; the most widely accepted mechanisms could be divided into four steps [8, 10, 15 and 24]. The first step is the dissolution of CO_2 in the aqueous solution to form the various reactive ions.

2.1.1 Dissolution of CO_2in the aqueous solution

Gaseous CO_2 dissolves in water:

$$CO_2\,(g) \leftrightarrow CO_2\,(aq) \qquad 2.1$$

Dissolved $CO_{2\,(aq)}$ will hydrate to form carbonic acid:

$$CO_2\,(g) + H_2O\,(l) \rightarrow H_2CO_3\,(aq) \qquad 2.2$$

The carbonic acid $H_2CO_{3\,(aq)}$ will dissociate and give off a proton and a bicarbonate ion:

$$H_2CO_3\,(aq) \rightarrow HCO_3^-\,(aq) + H^+\,(aq) \qquad 2.3$$

The bicarbonate ion will also dissociate to release another proton and carbonate ion:

$$HCO_3^-\,(aq) \rightarrow CO_3^{2-}\,(aq) + H^+\,(aq) \qquad 2.4$$

2.1.2 Transportation of reactants from bulk to surface

The second step is the transportation of these reactants to the metal surface.

$$H_2CO_3\,(aq)\,(bulk) \rightarrow H_2CO_3\,(aq)\,(surface) \qquad 2.5$$

$$HCO_3^-\,(aq)\,(bulk) \rightarrow HCO_3^-\,(aq)\,(surface) \qquad 2.6$$

$$H^+\,(aq)\,(bulk) \rightarrow H^+\,(aq)\,(surface) \qquad 2.7$$

2.1.3 Electrochemical reactions (Radox reaction)

The third step involves the electrochemical reactions which taking place at the metal surface. This reaction can be separated into anodic and cathodic half reactions, with both reactions happening simultaneously at the metal surface which called the radox reaction.

The anodic dissolution of iron is given by:

$$Fe\ (s) \rightarrow Fe^{2+}\ (aq) + 2e^- \qquad 2.8$$

The cathodic reaction involves two reactions depending on the pH. At a pH lower than 4, the proton (H^+) reduction is the dominant cathodic reaction, while at a pH higher than 4, the dominant reaction is the reduction of carbonic acid.

Proton reduction:

$$2H^+\ (aq) + 2e^- \rightarrow H_2\ (g) \qquad 2.9$$

Carbonic acid reduction:

$$2H_2CO_3\ (aq) + 2e^- \rightarrow H_2\ (g) + 2HCO_3^-\ (aq) \qquad 2.10$$

$$2HCO_3^-\ (aq) + 2e^- \rightarrow H_2\ (g) + 2CO_3^{2-}\ (aq) \qquad 2.11$$

At high overpotential, the dominant cathodic reaction changes to direct reduction water:

$$2H_2O\ (l) + 2e^- \rightarrow 2OH^-\ (aq) + H_2\ (g) \qquad 2.12$$

2.1.4 Transportation of products from surface to bulk

The forth step is the transportation of the corrosion products to the bulk of the solution. These can be shown as:

$$Fe^{2+}(aq)\ (surface) \rightarrow Fe^{2+}\ (aq)\ (bulk) \qquad 2.13$$

$$CO_3^{2-}\ (aq)\ (surface) \rightarrow CO_3^{2-}\ (aq)\ (bulk) \qquad 2.14$$

When the concentration of Fe^{2+} and CO_3^{2-} ions exceed the solubility limit, they combine to form solid iron carbonate layers according to:

$$Fe^{2+}\ (aq) + CO_3^{2-}\ (aq) \leftrightarrow FeCO_3\ (s) \qquad 2.15$$

The properties and morphology of the solid iron would influence the corrosion rate significantly.

The overall electrochemical reaction of CO_2 corrosion is given by:

$$Fe\ (s) + CO_2\ (g) + H_2O\ (l) \rightarrow FeCO_3\ (s) + H_2\ (g) \qquad 2.16$$

The schematic representations of the reactions are shown below;

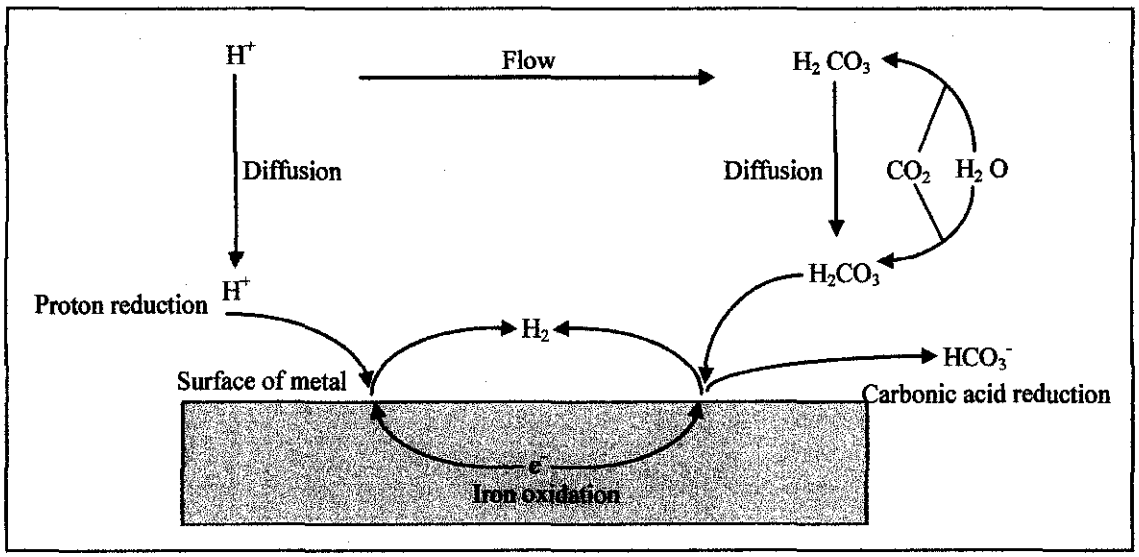

Figure 2.1: Simple model for CO_2 corrosion model. (Linter and Burstein, 1998) [6]

Figure 2.1 shows the schematic representations of CO_2 corrosion mechanisms under multiphase flow conditions. The iron dissolves into the water the water to form ion Fe^{2+} and subsequently releasing the electron. The protons, H^+ have to diffuse from the bulk region through the boundary layer to the metal surface, while the transport flux of carbonic acid needs to reflect both diffusion of H_2CO_2 and hydration of CO_2 in the boundary layer. The diffusion of hydrogen ions and carbonic acid is a rate determining step.

2.2 Factors effecting CO_2 corrosion

The parameters that influence CO_2 corrosion of steels can be described according to 3 categories which are materials-related, medium-related and inter phase-related parameters. Interface-related parameters include temperature, flow rate and presence of scales. Materials-related parameters are alloy composition and microstructure. The influences of pH, CO_2 partial pressure, solution chemistry, and presence of oxygen belong to medium-related parameters. All parameters are interdependent and influence the CO_2 corrosion in different ways.

2.2.1 Effect of iron carbonates scales

In CO_2 environments the main end product of carbon steel corrosion is iron carbonate which forms on the steel surfaces if the supersaturation of $FeCO_3$ in the near-surface solution is sufficiently high (Dugstad, 1997) [3]. $FeCO_3$ precipitates when Fe^{2+} ions react with carbonate (CO_3^{2-}) and bicarbonate (HCO_3^-) ions in the solution. Therefore a high supersaturation of Fe^{2+} and CO_3^{2-}/HCO_3^- is necessary for the formation of protective films. Once the film is formed, it will remain protective at a much lower supersaturation [3]. To get a successful protection, the film must be adherent and cover the whole surface. Localized corrosion can occur if parts of the scale break down and cannot re-form. The iron carbonate film functions as physical barrier which retards the diffusive transfer of corrosive species and prevent further metal dissolution of the blocked steel surface.

The protective properties of the surface scale depend on the characteristics of the material (metal composition and microstructure) and the environmental conditions (temperature, CO_2 partial pressure, pH) (Schmitt and Horstemeier, 2006) [12]. The protectiveness of solid iron carbonate will also depend on the rate of precipitation (which is a strong function of temperature and supersaturation) and on the underlying corrosion. For high precipitation rates, and low corrosion rates, the protective iron carbonate is obtained and vice versa, low precipitation rates and high corrosion rates lead to formation of non-protective iron carbonate layers.

2.2.2 Effect of temperature

The temperature strongly influences the CO_2 corrosion due to its effect on the rate of protective iron carbonate layer formation.Corrosion rates generally increase with increasing temperature when no protective surface films are present [8]. Muñoz et al. studied on the mechanism of protective film formation shows at lower temperatures (ca. < 60 °C) the solubility of $FeCO_3$ is high and the precipitation rate is slow and protective films will not form unless the pH is increased [5]. In this temperature range the corrosion rate increases with temperatures up to an intermediate range of ca. 60–80 °C. Above 60°C the protectiveness of the iron carbonate layer increases with temperature due to the decrease of iron carbonate solubility and, thus, the corrosion rate is reduced (Fig.2.2). At temperatures above 110°C magnetite (Fe_3O_4) may form through direct reaction between steel [2] and water and at 130°C the steels are passivated.

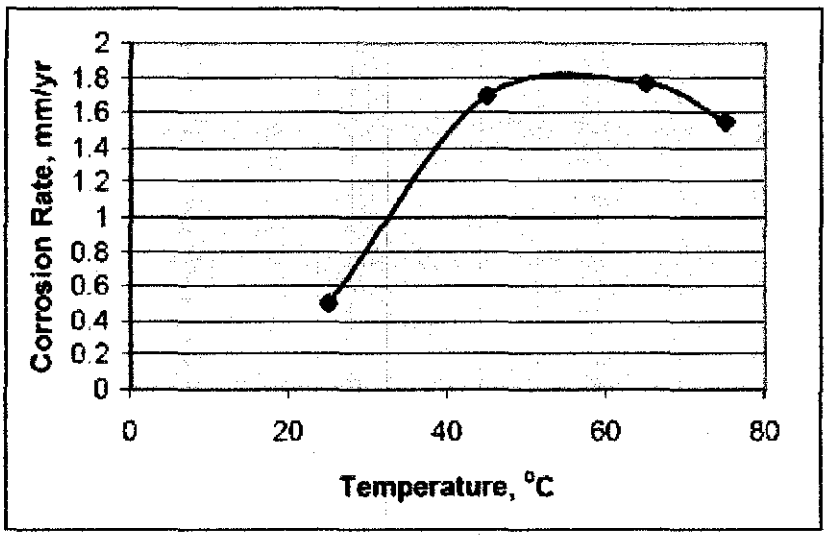

Figure 2.2: Corrosion rate of X70 steel as a function of temperature (3.5 % NaCl solution saturated with CO_2 at 0.07 MPa, stagnant conditions (Muñoz et al., 2005) [5]

2.2.3 Effect of flow

Under surface film forming conditions, there are two direct flow effects on the corrosion process. First, high flow rates may prevent the $FeCO_3$ film from growing on the metal surface. It can also damage or remove the existing film at some extremely high velocities [23]. High flow is also associated with high mass transfer rate which can help to accelerate the CO_2 corrosion process due to increased mass transfer. On the other hand, if the transport of the corrosive species is not fast enough to support the electrochemical reactions at the steel surface, then the corrosion rate is under mass transfer control.

2.2.4 Effect of alloy composition

The alloy composition of low alloy steel influences the corrosion rate where the highest effect is encountered with additions of chromium. The corrosion rate is significantly decreased with increasing Cr content [19]. In recent years the interest in low alloy steels with increased Cr content in the order of 3 to 5% Cr has increased due to the pressure to reduce CAPEX and OPEX in oil and gas production. An intermediate alloyed steel between API 5CT grade L80 and 13Cr steel would be of interest which offers improved corrosion resistance but stays with its costs close to API 5CT grade [21].

2.2.5 Effect of microstructure

The microstructure plays an important role in corrosion of carbon steel in CO_2-containingenvironments. Research by Ueda and Ikeda found that the materials with ferritic-pearlitic microstructure exhibit lower corrosion resistance and less localized-corrosion at temperature below 80°C than compared with martensitic microstructure [19].

2.2.6 Effect of CO_2 partial pressure

The formation of protective iron carbonate film on surface of carbon steel depends on conditions such as temperature, partial pressure, pH and Fe^{2+} concentration which are interrelated to each other. Under conditions favorable for protective film formation (low temperature and pH below 6)[19], increasing the partial pressure of CO_2 increases the acid ion (H_2CO_3) concentration and the solution become more corrosive. In film-forming conditions such as high pH; it gives the opposite effect of increasing the rate of iron carbonate precipitation and help reducing the corrosion rate. At atmospheric pressure, an increase in temperature gives rise to the contrasting effect of increasing the kinetics of precipitation and reducing the supersaturation.

Lin et al., conducted experiments at various CO_2 partial pressure and found that the thickness of iron carbonate film increases with the increases of CO_2 partial pressure until it reaches maximum at 6.89MPa [11]. Under such pressure, the corrosion rate of steel may have possibly reaches the maximum value and the large amount of $FeCO_3$ engenders the maximum value of the film thickness. Rhodes and Clark in their research found the relationship of the partial pressure of CO_2 and the corrosion rate of carbon steel as illustrated in Figure 2.3.

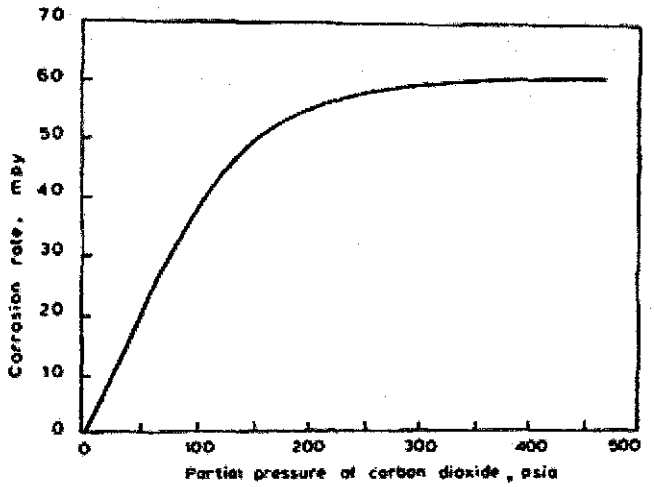

Figure 2.3: Relationship between corrosion rate of steel and partial pressure of CO_2. (Chilingar et al., 2008) [13]

It found that the relationship between corrosion rate of steel and partial pressure of CO_2. General rules of thumb for the corrosivity are [13]:

1. A partial pressure of CO_2 above 30psi usually indicates that corrosion will occur.
2. A partial pressure of 3 to 30psi indicates that corrosion may occur.
3. A partial pressure below 3psi indicates that corrosion generally is not serious.

2.2.7 Effect of pH

The pH represents the hydrogen ion concentration in a given solution. Changing in pH has very strong effect on the cathodic reactions which involves the reduction of H^+ ions (Chilinger et al., 2008) [13]. The cathodic reaction is strongly affected by pH where at a pH lower than 4, the proton (H^+) reduction is the dominant, while at a pH higher than 4, the *dominant reaction is the reduction of carbonic acid* [4]. *In general, an increase in pH will* decrease the corrosion rate under non-film-forming conditions [16]. In contrast, increase in pH will accelerate the precipitation of iron carbonate, $FeCO_3$.

$FeCO_3$ is relatively easy to grow on the metal surface under film-forming condition after reaching $FeCO_3$ supersaturation. This reaction was explained by Dugstad et al. [2]. In a close system, the dissolved iron concentration will increase until a balance is established where the release rate of Fe^{2+} is the same as the precipitation rate of $FeCO_3$. When Fe^{2+} is released, the double amount of bicarbonate forms according to eq. 2.17. As the result, the

pH will increase until the bicarbonate and carbonate concentration becomes so high (reaching $FeCO_3$ supersaturation) that solid $FeCO_3$ precipitates according to eq. 2.18. This condition decreases the corrosion rate of carbon steel due to the formation of protective corrosion product films.

$$Fe + 2H_2CO_3 \rightarrow Fe^{2+} + H_2 + 2HCO_3^- \qquad 2.17$$

$$Fe^{2+} + 2HCO_3^- \rightarrow FeCO_3\ (solid) + H_2CO_3 \qquad 2.18$$

When all the Fe^{2+} ions produced by corrosion precipitate as iron carbonate the pH will remain constant. In another study, Dugstad et al. proved experimentally that the pH is affected by the amount of dissolved corrosion product as shown in Figure 2.4 [2].

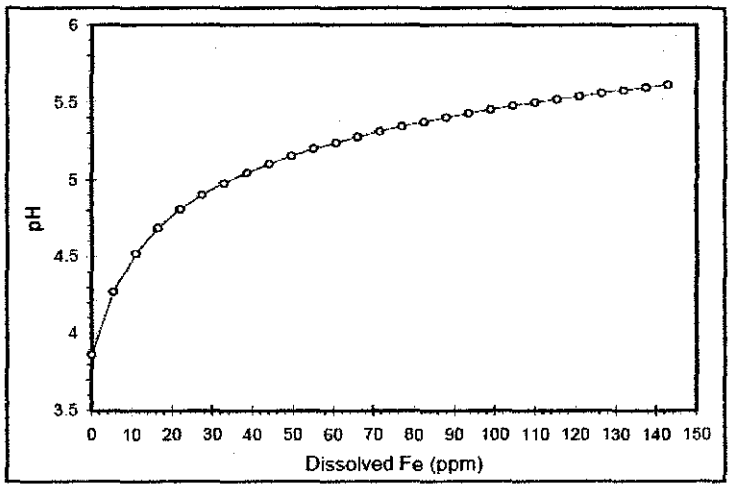

Figure 2.4: Relationship between pH and amount dissolved corrosion products (0.1 MPa CO_2 and temperature 40°C). (Dugstad et al., 2006) [2]

2.2.8 Effect of Fe^{2+} concentration

The rate of deposition of protective corrosion product film ($FeCO_3$) depends on the precipitation rate of Fe^{2+} and CO_3^{2-}. When an iron carbonate layer forms on the surface of metal, it acts as a diffusion barrier and prevents the metal from further corrosion, subsequently; the corrosion rate is reduced [4]. The driving force for precipitation is the supersaturation of $FeCO_3$ [4]. The precipitation of iron carbonate takes place when it reaches the solubility limit of ion Fe^{2+} and CO_3^{2-}. The precipitation of $FeCO_3$ is a very slow process and a high degree of supersaturation of iron carbonate is necessary in order to form a protective layer of iron carbonate. Dugstad showed experimentally that the solubility of $FeCO_3$ is strongly dependent on the pH and CO_2 partial pressure [4].

2.2.9 Effect of oxygen

Oxygen in CO_2 systems exhibits a strong effect on the corrosion rate and facilitates the formation of localized attack. Based on the research by Martin on the corrosion consequences of oxygen entry into both sweet and sour systems found that that the corrosion rate in CO_2 system is accelerated in the presence of oxygen by 0.5 mm/year per ppm of oxygen at medium velocity and ambient temperature [22]. He suggested that the mechanism is consistent with a change in surface corrosion product, which accelerates H_2CO_3 reduction [22].

2.3 CO_2 corrosion in the present of Ca^{2+}

In oil and gas fields, the formation water contains many mineral ions such as Ca^{2+} and Mg^{2+}. Present of Ca^{2+} can affect the corrosion rate because this cation reacts with carbonic acid and deposit calcium carbonates, $CaCO_3$. This codeposition of calcium carbonates, $CaCO_3$ and iron carbonates, $FeCO_3$ enhances the scale formation and, hence, reduces the corrosion rates [20]. Present of Ca^{2+} and CO_3^{2-} lead to precipitation of carbonate scale, $CaCO_3$ when super saturation occur. Once, the solubility capacity is exceeded, the carbonate scale, $CaCO_3$ will precipitate from solution as solid on metal surface. Jiang et al. found that the corrosion product film in 3%NaCl + 1.5%$CaCl_2$ solution mainly composed of $CaCO_3$, $FeCO_3$ and Fe_3C [26]. Ca^{2+} can influence the susceptibility of pitting corrosion. Jiang et al. investigated the effect of Ca^{2+} on pitting corrosion in CO_2 environment. The results indicated that in the solution containing Ca^{2+}, the initiation period of pitting corrosion is longer than the solution without Ca^{2+} [26]. A thicker corrosion product scale formed due to present of $CaCO_3$ scale provides a greater degree of corrosion protection by decreasing the transport rate of reactive species to the metal surface. Other research by Ueda et al. found that the corrosion rates of carbon steels in $CaCl_2$ solutions were smaller than those in 5% NaCl + 2.5meq/l $NaHCO_3$ solution with same pH, but the steels showed higher localized attack [20].

In laboratory experiment, Ca^{2+} normally is added to the solution as $CaCl_2$. Cl^- is widely thought has significant effect on general and localized corrosion [14]. Fang et al. studies on the effect of high salinity brines on general CO_2 corrosion concluded that Cl^- accelerate general corrosion [14]. However, in CO_2 corrosion studies with the present of Ca^{2+}, Ca^{2+} and Cl^- are simultaneously added by the addition of $CaCl_2$ into NaCl solution to simulate the formation water, it is not known which one effect the CO_2 corrosion. Ding et al. claimed that the effect of Cl^- could be ignored since there was a lot of Cl^- existed as NaCl [7]. In other research by Jiang et al., they considered the effect of Cl^- by conducting the tests at constant Cl^- concentration in order to know if present of Ca^{2+} has effects on CO_2 corrosion or not [26]. The concentration of Ca^{2+} in formation water varies depend upon the field location. For example, in peninsular Malaysia fields, the range of Ca^{2+} concentration in formation water is from 7000ppm to 30000ppm [1].

2.4 Laboratory works related to CO_2 corrosion for the measurements of severity of CO_2 corrosion

In the last fifty year, extensive experimental studies on the mechanisms of CO_2 corrosion and the factors affecting the corrosion rate have been carried out. Corrosion of carbon steel in oil and gas systems is governed by a complex mixture of various mechanisms. A large number of parameters are involved and they affect the corrosion mechanisms differently. The most important parameters are related to material properties, fluids chemistry and operational conditions. To simulate all the field parameters in laboratory tests is impossible (Dugstad et al., 2006) [2]. The challenge is therefore to simplify the system without losing control of the main controlling parameters and without switching to other corrosion controlling mechanisms [2].

Mechanism of CO_2 corrosion can be investigated through electrochemical reactions at the metal-solution interface. The most common method which used electrochemical reactions is Linear Polarization Resistance (LPR) and Electrochemical Impedance Spectroscopy (EIS). In early studies, weight loss corrosion tests were used in order to determine corrosion rate. Modern instrumental techniques such Scanning Electron Microscopy (SEM), X-Ray Photoelectron Spectroscopy (XPS), Auger Electron Spectroscopy (AES) and Ion Mass Spectroscopy (SIMS) was used to evaluate the corrosion products.

Linear Polarization Resistance (LPR) monitoring is an effective electrochemical method of measuring corrosion. Monitoring the relationship between electrochemical potential and current generated between electrically charged electrodes in a process stream allows the calculation of the corrosion rate. LPR is most effective in aqueous solutions, and has proven to be a rapid response technique [17].

Electrochemical Impedance Spectroscopy (EIS) also known as AC impedance spectroscopy is a non destructive electrochemical method that is used to evaluate the electrochemical properties of electrode and electrode/electrolyte interface. During EIS experiments, a small amplitude ac signal is applied to the system being studied. Therefore, it is a non-destructive method for the evaluation of a wide range of materials, including coatings, anodized films and corrosion inhibitors. It can also provide detailed information of the systems under examination; parameters such as corrosion rate, electrochemical

mechanisms and reaction kinetics, detection of localized corrosion, can all be determined from these data [9].

Corrosion tests to investigate the mechanisms of CO_2 corrosion should be reproducible and reliable. Corrosion tests may be classified as the simulated laboratory test and field test. Laboratory tests can be classified as long-term or accelerated short-term test. Long-term laboratory test are usually used in the materials selection process where the test is conducted at simulated field conditions. In accelerated short-term tests, one or several factors affecting the corrosion rate are made severe to speed up the corrosion process. This type of test is done in controlled conditions and is useful in quality control of material or protective coatings.

In laboratory scale system, the corrosion tests have been done by using cylinder electrode cell and the laboratory scale flow loop. A schematic representation of a typical glass cell is shown in Figure 2.5. By using rotating cylinder electrode cell, flow condition (laminar, turbulent and transitional flow) can be simulated using a variety of electrode geometries whereas pipe flow loop incorporating a test cell configuration enabling electrochemical investigations under fully-developed fluid flow fields, from laminar, transient to turbulent flow regimes.

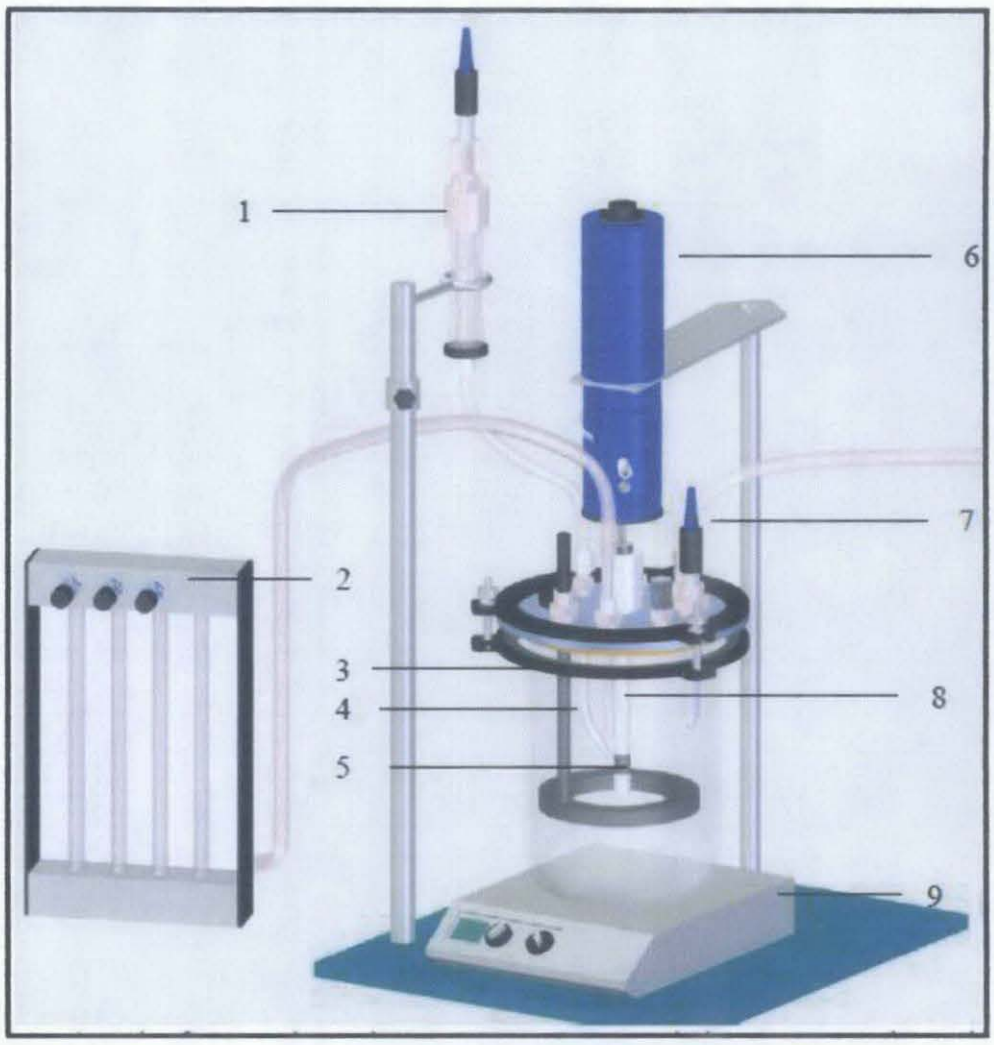

1- Ag/AgCl reference electrode; 2- gas rotameter; 3- platinum counter electrode; 4- luggin capillary; 5-X-65 carbon steel working electrode; 6-shaft; 7- pH probe; 8- bubbler; 9- hot plate.

Figure 2.5: Schematic of the glass cell setup (Design one)

Lab tests generally yield difference results compared with the field tests. This is not only due to generally shorter exposure time. This must be also attributed to the experimental problem to keep certain experimental conditions constant over longer period of time. The evaluation of various parameters that govern the corrosion mechanisms was presented by Dugstad et al. in their research on the limitations and challenges of corrosion testing in multiphase flow [2]. They categorized these parameters into two categories, easy to control and complicated. Table 2.1 shows their findings.

Table 2.1: The parameters that affecting the corrosion rate and the execution of lab experiments. (Dugsted et al., 2006) [2]

Parameters	**Easy to control**	**Complicated to control**	**Comments**
Temperature	X		
CO_2	X		Consumed and has to be replenished
HAc		X	Consumed, sensitive to pH, low concentrations are difficult to control
Flow rate	X		
Flow regime		X	Scale up problems
Oil/water wetting		X	Difficult to run live oil experiments
Oil properties		X	Large differences between model oils, stabilized oil and live oil.
Steel composition	X		Use the same batch of steel as in the field if possible.
Water chemistry:			
Fe^{2+}		X	Produced and has to be removed
Ca^{2+}, Sr^{2+}, Ba^{2+}		X	Consumed and has to be replenished
Other salts	X		
Steel surface properties		X	Mill scale, rust, corrosion films
Operational parameters		X	Shut down, changing parameters
pH	X		Depending on the buffering capacity of the water

CHAPTER 3

METHODOLOGY

3.1 Project Flow

Figure 3.1 shows the details of project flow.

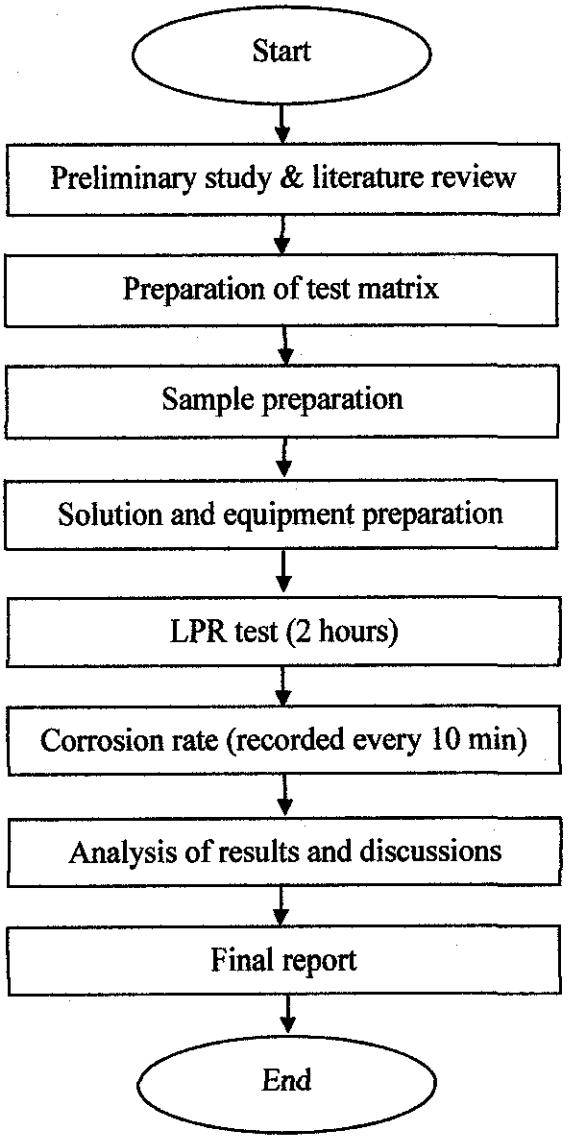

Figure 3.1: Project flow chart

The project started with the preliminary study and literature review on CO_2 corrosion mechanism; to look at the factors that influence CO_2 corrosion by focusing on the effect of Ca^{2+}. The study also covers on the available experimental methods in CO_2 corrosion.

Next, all information related to the project is gathered in a proper documentation. Detail review and analysis on the previous work by other researchers has been conducted to see what have been done so far on this area of study. Based on the review, the test matrix was designed for experimental works.

Linear Polarization Resistance (LPR) test was carried out to determine the corrosion rate. The research was done at Ca^{2+} concentration of peninsular Malaysia offshore field from 7000ppm to 20000ppm Cl^- [1]. The test temperatures were set at 50°C and 80°C to simulate real field condition. Carbon steel (X-52) sample from transportation pipeline was used as test specimen and its chemical composition is shown in Table 3.2. Baseline tests were conducted in the absence of Ca^{2+} which would serve as a means of comparison for tests with Ca^{2+}. pH, CO_2 pressure and Cl^- concentration are held constant so that the results solely reflect the different in concentration. Each test was conducted for 2 hours and the result was recorded every 10 minutes.

Lastly, the research is documented and compiled to be a proper Final Year Project report dissertation.

3.2 Gantt chart

3.2.1 Final Year Project 1 (FYP1)

	Week													
Task/Activity	1	2	3	4	5	6	7	8	9	10	11	12	13	14
Selection of FYP topic		■					MIDSEM BREAK							
Preliminary research works			■	■										
Submission of preliminary report						■								
literature review			■	■	■	■			■	■	■	■		
Seminar					■									
Progress report submission									■					
Design laboratory works									■	■	■	■		
Preparation of final report												■	■	■
Preparation of final presentation													■	■
Interim final report submission														■
Oral presentation														■

Figure 3.2: Gantt chart for FYP1

3.2.2 Final Year Project 2 (FYP2)

	Week														
Task/Activity	1	2	3	4	5	6	7	8	9	10	11	12	13	14	15
Design laboratory works	■	■													
Booking of laboratory	■	■													
Preparation of specimen		■													
Experimental work commences			■	■	■	■	■	■	■						
Data analysis							■	■	■	■	■				
Preparation of progress report										■					
Preparation of paper/journal										■	■				
Preparation of seminar												■	■		
Preparation of poster												■	■		
Preparation of final report									■	■	■	■	■		
Preparation of oral presentation														■	■

Note: Week 1 and 2 is during the semester break (10-23 January 2011)

Figure 3.3: Gantt chart for FYP2

3.3 Experimental Details

3.3.1 Test Matrix

To determine the general effects of Ca^{2+} concentration on carbon steel corrosion in a CO_2 saturated environment, the following series of tests were planned under difference concentration of Ca^{2+}. The reference (baseline) test was conducted first and then different concentrations of Ca^{2+} were varied. Table 3.1 shows the test matrix of the experiment.

Table 3.1: Test matrix

Parameter	Value			
Steel type	Carbon steel, X-52			
Purging Gas	CO_2			
Temperature (°C)	50, 80			
pH	4			
Cl^- concentration	Constant			
Experiment duration (hrs)	2			
Ca^{2+} concentration (ppm)	**0**	**7000**	**10000**	**20000**
Solution	60g/L NaCl	39.58g/L NaCl + 19.38g/L $CaCl_2$	30.84g/L NaCl + 27.69g/L $CaCl_2$	1.67g/L NaCl + 55.38g/L $CaCl_2$

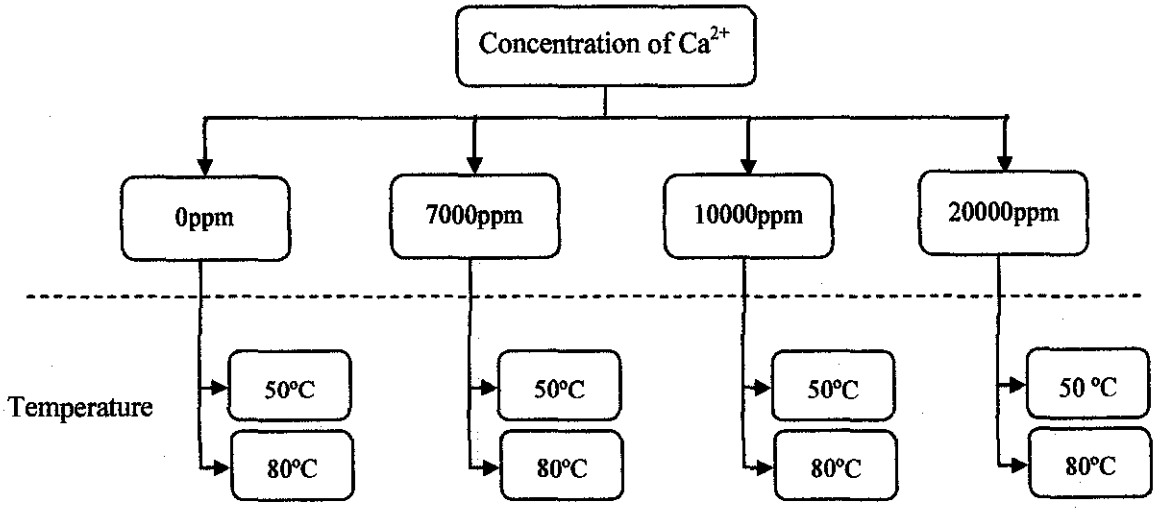

Figure 3.4: Test Matrix

3.3.2 Material

Mild steel X-52 samples with the chemical composition shown in Table 3.2 were used for this study.

Table 3.2: Composition of mild steel X-52

Nominal Composition, Weight %							
C	Mn	Si	P	S	Nb	V	Fe
0.15	1.25	0.2	0.027	0.026	0.04	0.05	Balance

3.3.3 Solution

The experiments were carried out in NaCl + $CaCl_2$ solution. Ca^{2+} concentration in the simulated solution was set up at 7000, 10000 and 20000 ppm. Cl^- concentration was held constant at 36397.54 ppm. The amount of NaCl and $CaCl_2$ required were calculated as follow:

(A) Calculation of $CaCl_2$

In basis of 1 Liter solution:

1. The conversion of required Ca^{2+} concentration (in $CaCl_2$) to mol is as follow:

$$\textbf{mol of } Ca^{2+} = \frac{Ca^{2+}\text{ concentration required in } CaCl_2\text{ (ppm)} \times 10^{-3}\,\frac{g}{mg}}{40.078\,\frac{g}{mol}} \qquad 3.1$$

2. The number mol of $CaCl_2$ required according to the following equation:

$$1\text{ mol } CaCl_2(s) \leftrightarrow 1\text{mol } Ca^{2+}(aq) + 2\text{ mol } Cl^-(aq)$$

3. The ratio of the mol are as follow

Mol ratio	
$CaCl_2$	Ca^{2+}
1	1

4. The mass of $CaCl_2$ required:

$$\text{Mass of } CaCl_2 = \text{mol of } CaCl_2 \times 110.9834\,\frac{g}{mol} \qquad 3.2$$

5. The concentration of Cl^- in $CaCl_2$ is according to the mol ratio as shown below

Mol ratio	
Ca^{2+}	Cl^-
1	2

6. The concentration of Cl^- in $CaCl_2$ was calculated as follow

$$\textbf{Concentration of } Cl^- \text{ (ppm)} = \text{Mol of } Cl^- \times 35.4527 \frac{g}{mol} \times 10^3 \frac{mg}{g} \qquad 3.3$$

(B) Calculation of NaCl

In basis of 1 Liter solution:

1. The concentration of Cl^- in the solution was set at constant concentration of 36397.54 ppm.

   Concentration of Cl^- in $CaCl_2$ (ppm) + concentration of Cl^- in NaCl (ppm) = 36397.54 ppm 3.4

2. The conversion of required Cl^-concentration (in NaCl) to mol is as follow:

$$\textbf{mol of } Cl^- = \frac{Cl^- \text{ concentration required in NaCl (ppm)} \times 10^{-3} \frac{g}{mg}}{35.4527 \frac{g}{mol}} \qquad 3.5$$

3. The number mol of NaCl required according to the following equation:

$$1 \text{ mol NaCl (s)} \leftrightarrow 1 \text{ mol } Na^+\text{(aq)} + 1 \text{ mol } Cl^-\text{(aq)}$$

4. The ratio of the mol are as follow

Mol ratio	
NaCl	Cl^-
1	1

5. The mass of a NaCl required:

$$\textbf{Mass of NaCl} = \text{mol of NaCl} \times 58.4527 \frac{g}{mol} \qquad 3.6$$

Table 3.3 shows the summary of NaCl and $CaCl_2$ required.

Table 3.3: Calculated amount of NaCl and $CaCl_2$

Concentration of Ca^{2+} (ppm)	**0**	**7000**	**10000**	**20000**
Solution	60g/L NaCl	39.58g/L NaCl + 19.38g/L $CaCl_2$	30.84g/L NaCl + 27.69g/L $CaCl_2$	1.67g/L NaCl + 55.38g/L $CaCl_2$

3.3.4 Linear Polarization Resistance (LPR)

Linear Polarization Resistance (LPR) uses linear approximation of polarization behavior at potentials near the corrosion potential. The corrosion current density (i_{corr}) is given by Stern and Geary equation

$$i_{corr} = \frac{\Delta E}{\Delta L} = \frac{B}{R_p} \qquad 3.7$$

where

R_p = Resistance polarization (ohm-cm^2)

B = The Stern-Geary constant

$$\text{where } B = \frac{b_a b_c}{2.303(b_a+b_c)} \qquad 3.8$$

and where b_a and b_c is the Tafel slopes for anodic and cathodic curves repectively. The Stern-Geary, B is approximated as 25mV for all pH.

The corrosion rate can be determined by using Faraday's law:

$$\text{Corrosion rate } \left(\frac{\text{mm}}{\text{year}}\right) = \frac{315 Z i_{corr}}{\rho n F} \qquad 3.9$$

where

i_{corr} = corrosion current density (μA/cm^2)

ρ = Density of iron, 7.8g/cm^3

F = Faraday's constant, 96500 C/mole

Z = Atomic weight (g/mol)

n = number of exchange electron

3.3.5 Experimental work flow

3.3.5.1 Preparation of Specimen

1. Two specimens were prepared with surface area of $0.64cm^2$ and $0.67cm^2$.
2. The samples were spot welded with copper wire.
3. The specimen was mounted with epoxy by cold mounting and the specimen surface was then polished to a 600-grade finish using silicon carbide paper.
1. The specimen was degreased and rinsed with deionizer water and ethanol prior to immersion.

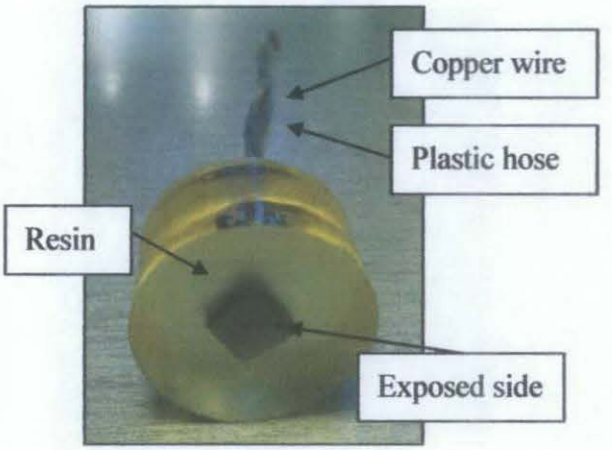

Figure 3.5: Working electrode

3.3.5.2 Preparation of electrolyte

1. The solutions as shown in table 3.4 were prepared.

Table 3.4: Experimental solutions

Experiment	**1**	**2**	**3**	**4**
Solution	60g/L NaCl	39.58g/L NaCl + 19.38g/L $CaCl_2$	30.84g/L NaCl + 27.69g/L $CaCl_2$	1.67g/L NaCl + 55.38g/L $CaCl_2$

2. 1 bar of CO_2 gas was continuously purged into solutions until the CO_2 is saturated in the solutions.

Note:

1. CO_2 gas was continuously purged for at least one hour prior to the expose of electrodes.
2. The electrolyte is saturated with CO_2 when the pH of the solution is nearly 3.8, which is the saturation pH of CO_2 in the solution at room temperature (≈25°C).

3.3.5.3 Laboratory set-up

Experiments were done under static condition using electrochemical measurements base on three-electrode system, using a potentiostat with a computer control system. All the experiments were carried out in standard 1 liter glass cell. The required test temperature was set through the hot plate. The reference electrode was Ag/AgCl and the auxiliary electrode was graphite electrode. The pH of the solution was monitored using pH-meter METTLER-TOLEDO Model 320, which calibrated using standard buffer solutions. The required temperature was monitored using thermometer. The set-up of the experiment is shown in Figure 3.6.

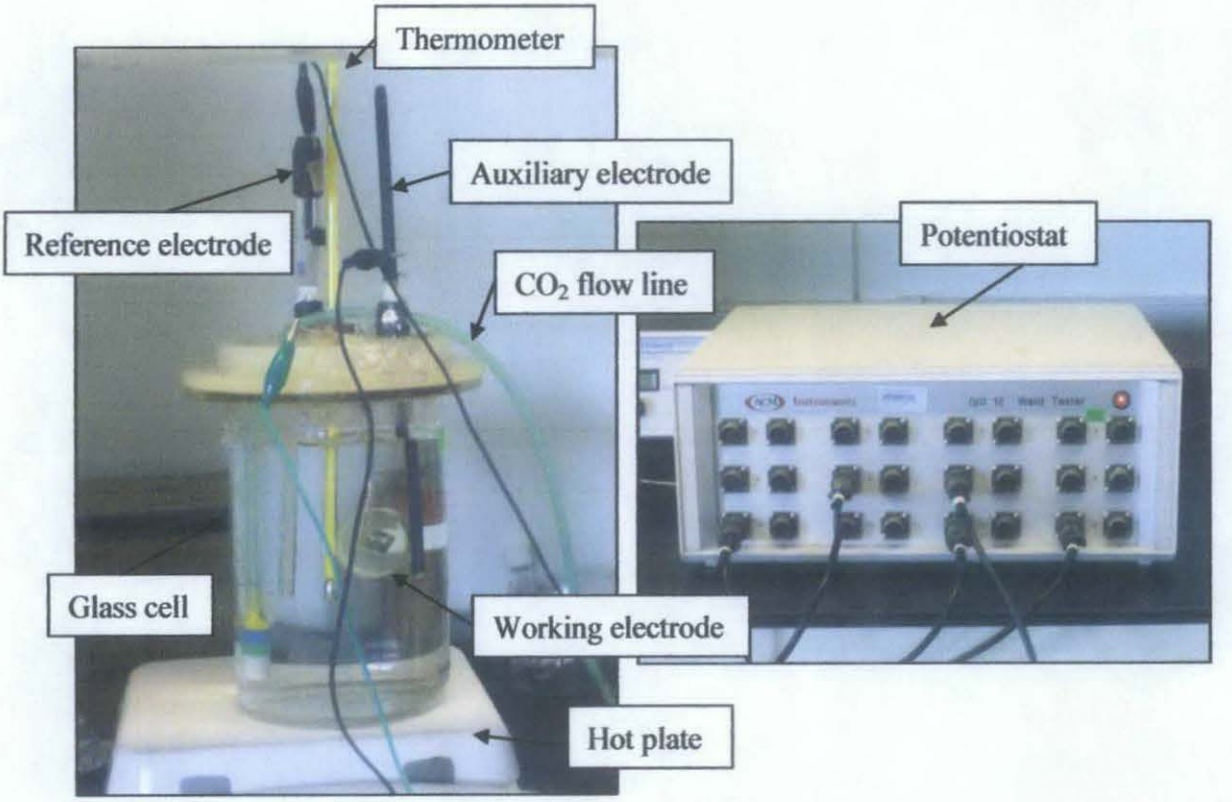

Figure 3.6: Experimental setup

3.3.5.4 Experimental Procedures

1. The working electrolytes were prepared as per describe in section 3.3.5.1.
2. The test solution was prepared as per describe in section 3.3.5.2.
3. The equipments for laboratory test was set up as per describe in section 3.3.5.3.
4. The required test temperature of 25°C was set through the hot plate and was monitored using thermometer. Once the temperature of the experiment achieved, the pH of the solution is adjusted to 4.0 by adding deoxygenated sodium bicarbonate solution, $NaHCO_3$. pH of the solution was checked using pH-meter METTLER-TOLEDO Model 320.
5. After all desired experimental conditions have been achieved; the three-electrode system was connected to ACM Instruments Version 5. Gill 12 Weld Tester-Sequencer and Core Running software were run on computer system.
6. Long-term-LPR sweep measurements were performed by measuring the corrosion potential of exposed specimen and subsequently sweeping from -10mV to +10mV with a sweep rate of 10mV/min.
7. 12 measurements were recorded with the time delay between reading is at 10 minutes.
8. As the measurement completed, the temperature of the solution was increased to 80°C. Then, steps 6 - 7 were repeated.

CHAPTER 4

RESULTS

4.1 Linear Polarization Resistance Test

Linear Polarization Resistance (LPR) tests were carried out at a constant pH of 4.0 and temperature of 50°C and 80°C in the presence of CO_2. Baseline tests were conducted in the absence of Ca^{2+} which serves as a means of comparison for tests with Ca^{2+}. The Ca^{2+} concentrations were increased from 7000 ppm up to 20000 ppm to allow observation of the Ca^{2+} effect. The Cl^- concentration was set constant to distinguish the effect of the Ca^{2+} from the effect of Cl^-. Reproducibility of results is ensured by accurate preparation of test specimens and test solutions. **It is necessary to point out that the experiments were repeated in order to check the consistency of results.**

4.1.1 Test results

4.1.1.1 Concentration of Ca^{2+}: 0 ppm at 50°C

From Figure 4.1, the corrosion rate found to be 2.35mm/year after 2 hours of exposure.

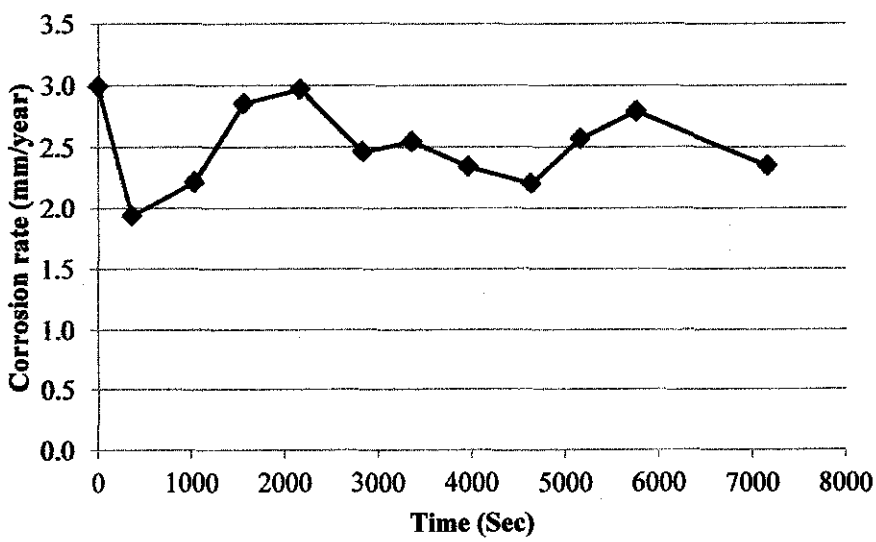

Figure 4.1: Corrosion rate of 0 ppm Ca^{2+} at 50°C

4.1.1.2 Concentration of Ca^{2+}: 0 ppm at 80°C

From Figure 4.2, the corrosion rate found to be 3.26mm/year after 2 hours of exposure.

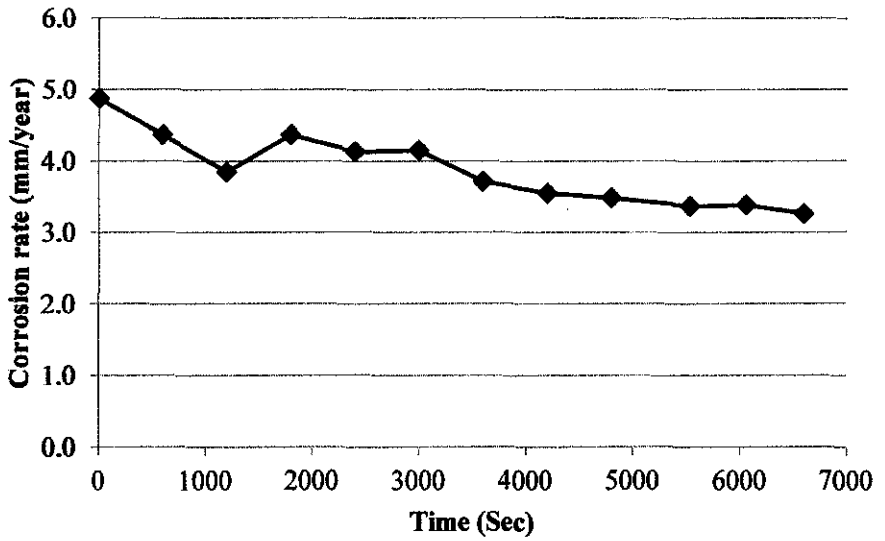

Figure 4.2: Corrosion rate of 0 ppm Ca^{2+} at 80°C

4.1.1.3 Concentration of Ca^{2+}: 7000 ppm at 50°C

From Figure 4.3, the corrosion rate found to be 0.41mm/year after 2 hours of exposure.

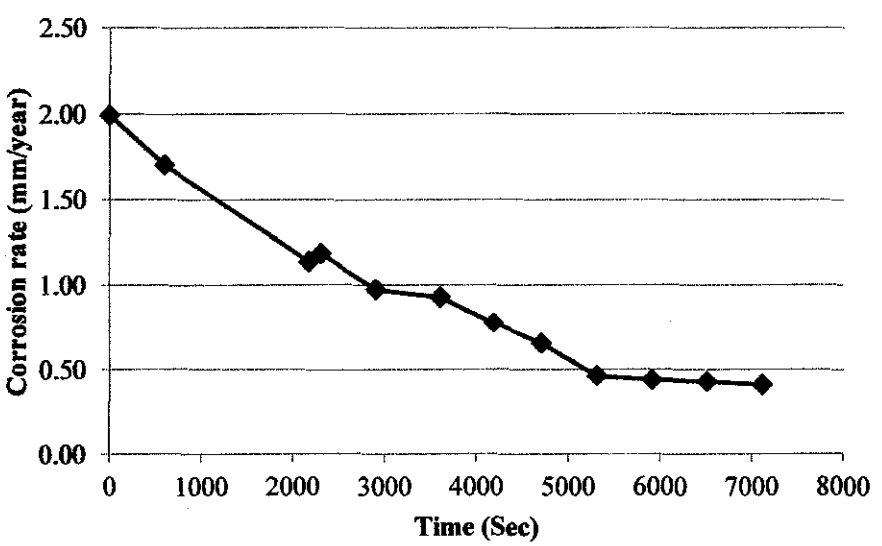

Figure 4.3: Corrosion rate of 7000 ppmCa^{2+} at 50°C

4.1.1.4 Concentration of Ca^{2+}: 7000 ppm at 80°C

From Figure 4.4, the corrosion rate found to be 0.545mm/year after 2 hours of exposure.

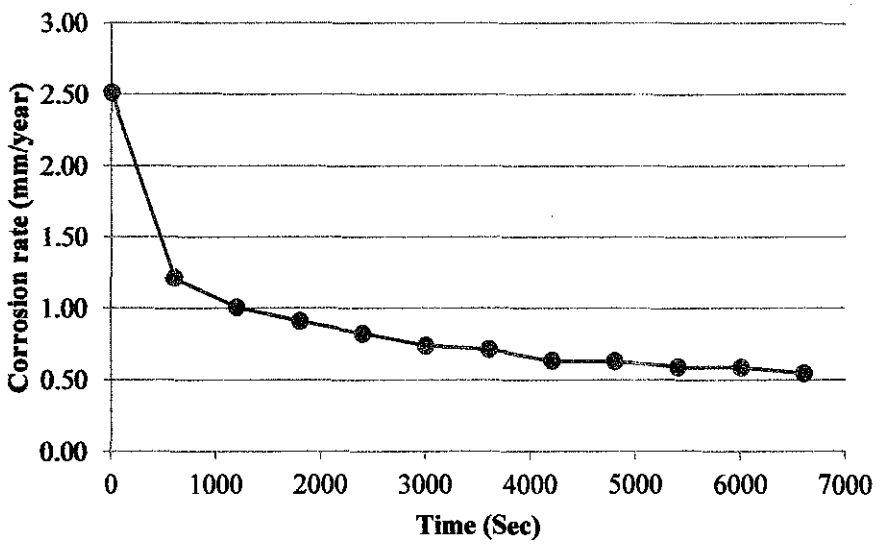

Figure 4.4: Corrosion rate of 7000 ppm Ca^{2+} at 80°C

4.1.1.5 Concentration of Ca^{2+}: 10000 ppm at 50°C

From Figure 4.5, the corrosion rate found to be 0.549mm/year after 2 hours of exposure.

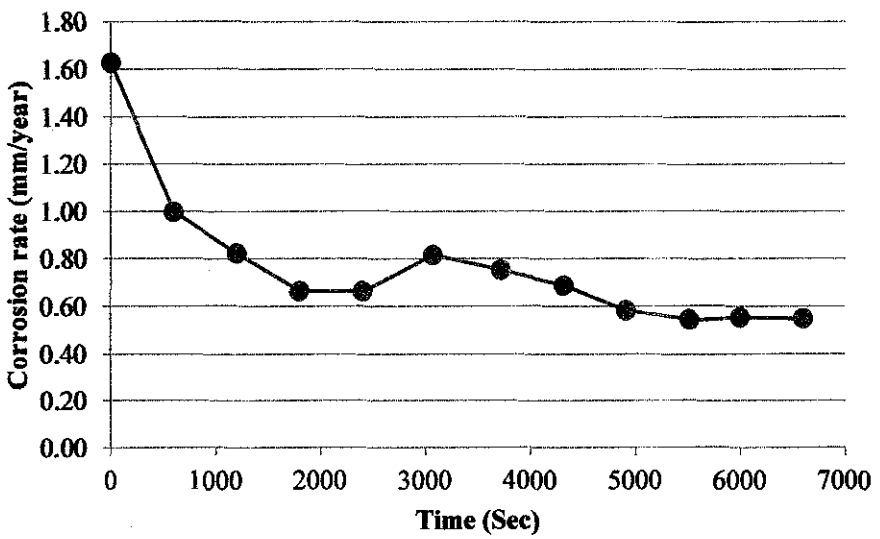

Figure 4.5: Corrosion rate of 10000 ppm Ca^{2+} at 50°C

4.1.1.6 Concentration of Ca^{2+}: 10000 ppm at 80°C

From Figure 4.6, the corrosion rate found to be 0.61mm/year after 2 hours of exposure.

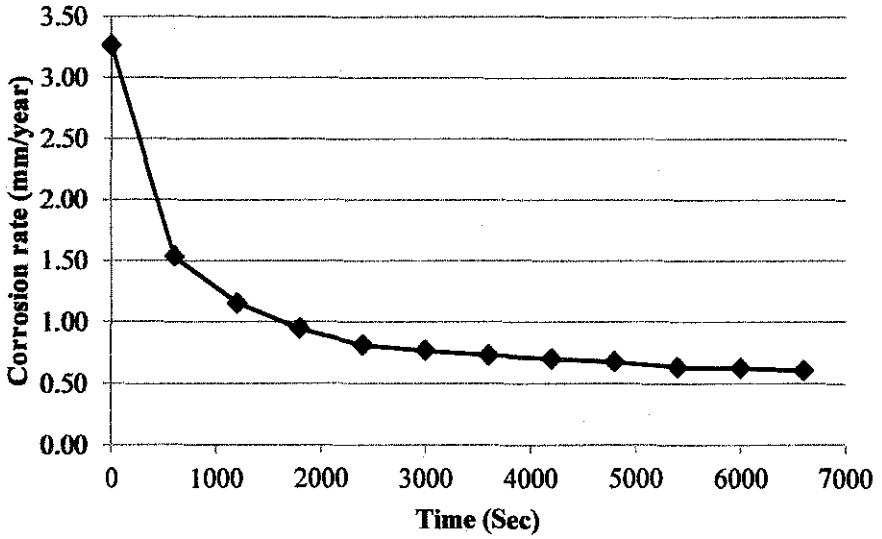

Figure 4.6: Corrosion rate of 10000 ppm Ca^{2+} at 80°C

4.1.1.7 Concentration of Ca^{2+}: 20000 ppm at 50°C

From Figure 4.7, the corrosion rate found to be 0.83mm/year after 2 hour

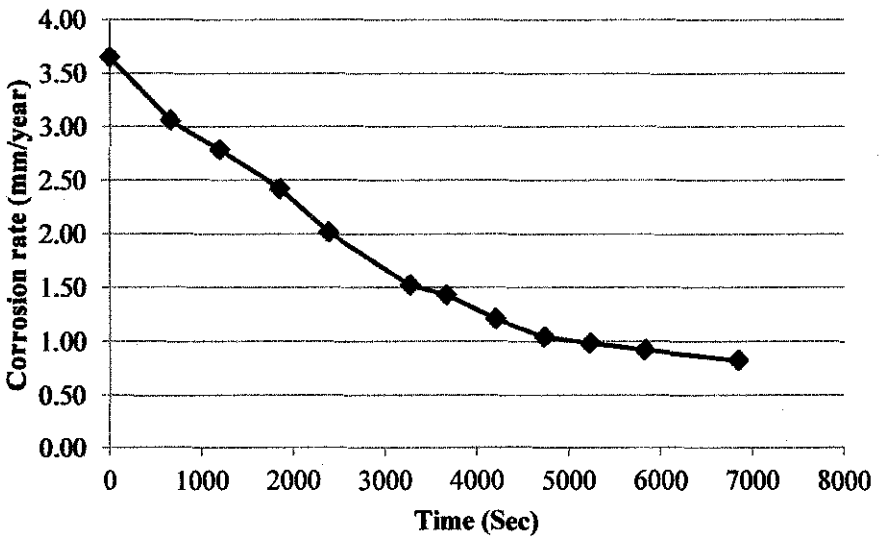

Figure 4.7: Corrosion rate of 20000 ppm Ca^{2+} at 50°C

4.1.1.8 Concentration of Ca^{2+}: 20000 ppm at 80°C

From Figure 4.8, the corrosion rate found to be 1.176mm/year after 2 hours of exposure.

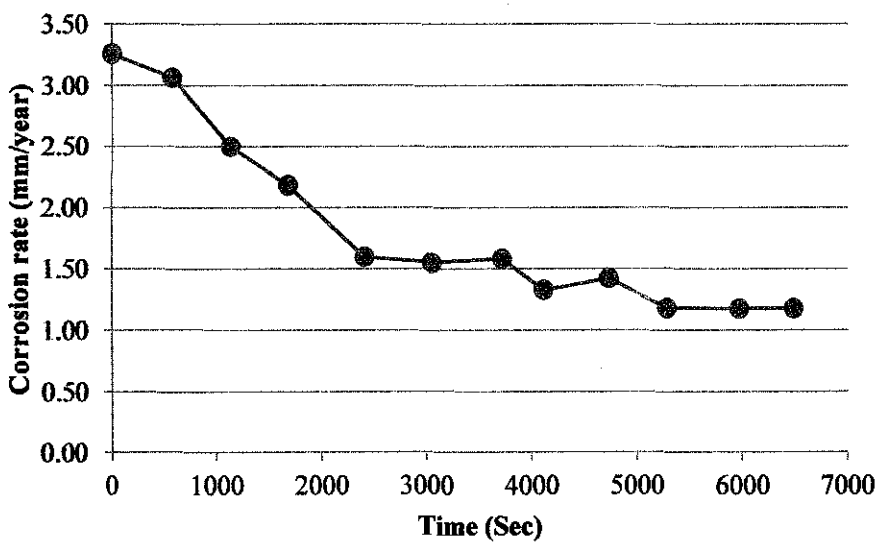

Figure 4.8: Corrosion rate of 20000 ppm Ca^{2+} at 80°C

4.2 Discussion

The corrosion rates of the carbon steel specimen exposed to various concentrations of Ca^{2+} after 2 hours of exposure, pH 4 and temperature of 50°C and 80°C at are shown in Table 4.1. The corrosion rates were taken after 2 hours of expose for the analysis of LPR test because the chemical reaction between the corrosion species in the solution is already stable at the end of two (2) hours. This could be explained by the plot of corrosion potential, E_{corr} versus immersion time as shown in Figure 4.9 and Figure 4.10. The corrosion potential, E_{corr} at 50°C and 80°C are stable after approximately 60 minutes.

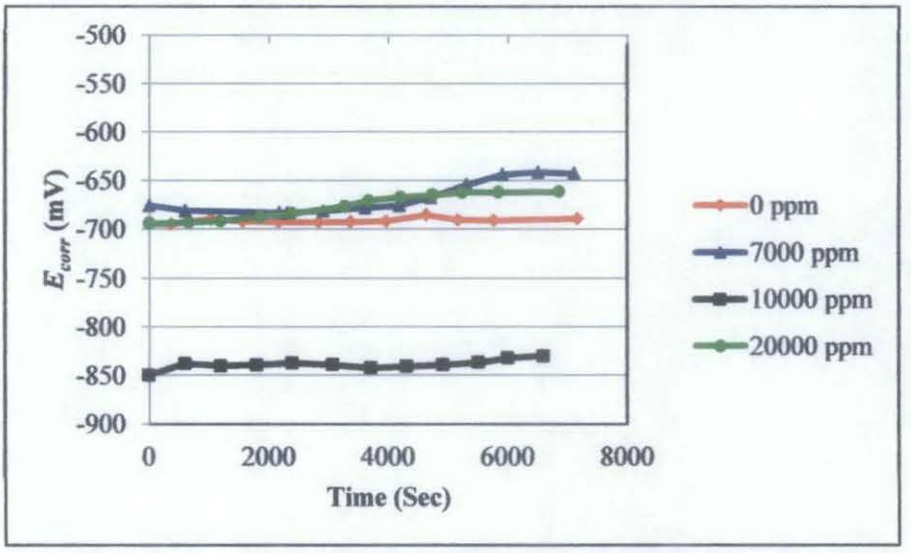

Figure 4.9: E_{corr} versus time at 50°C

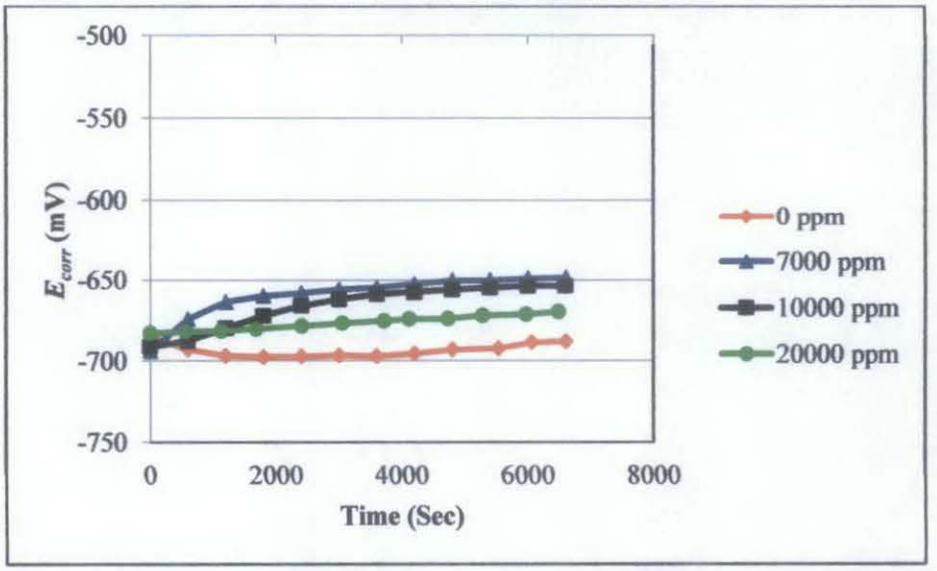

Figure 4.10: E_{corr} versus time at 80°C

Table 4.1: Corrosion rates at the end of 2 hours, pH 4, and temperature of 50°C and 80°C with various Ca^{2+} concentrations

Temperature, °C	Corrosion rates at different concentration of Ca^{2+}, ppm			
	Blank solution	7000	10000	20000
50	2.35	0.41	0.55	0.83
80	3.26	0.55	0.61	1.18

From Table 4.1, it can be observed that corrosion rates of both blank solutions (without Ca^{2+}) and with Ca^{2+} are influenced by concentration of Ca^{2+} and temperature. Therefore, the analysis of LPR test is divided into individual effect of Ca^{2+} concentration and temperature.

4.2.1 Effect of Ca^{2+} concentration

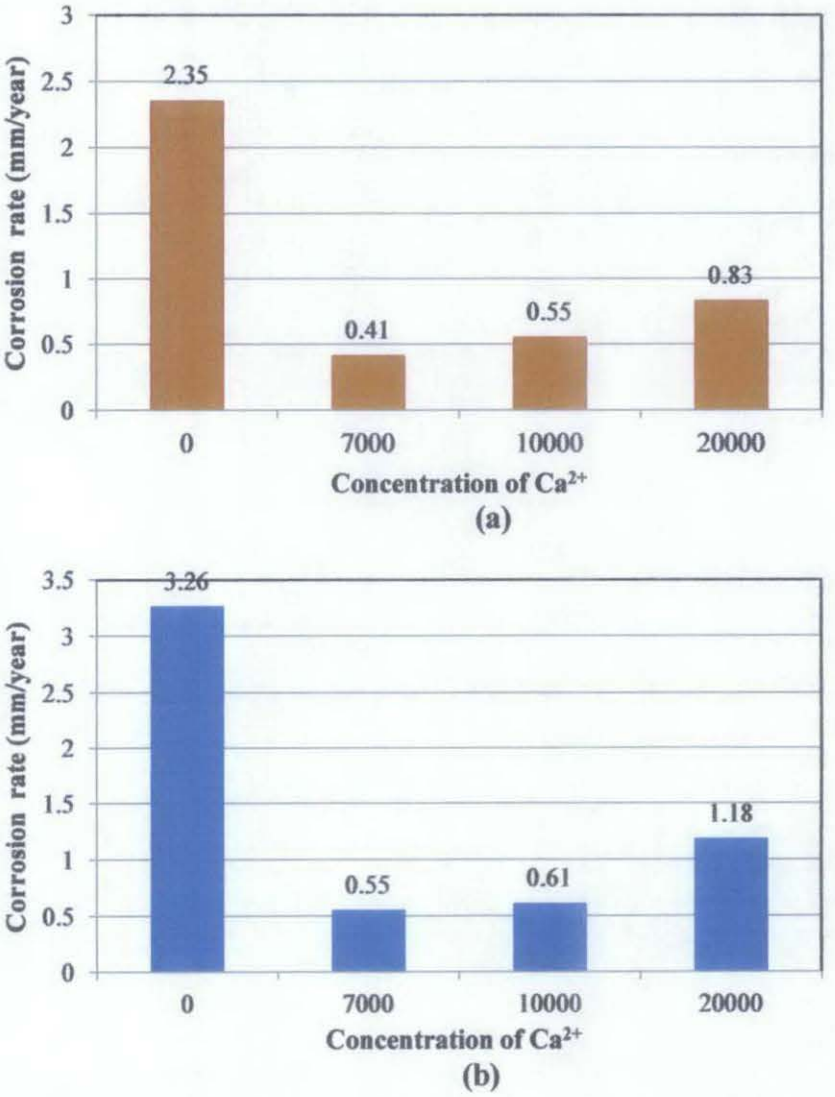

Figure 4.11: *Corrosion rate at various Ca^{2+} concentrations: (a) 50°C (b) 80°C*

From Figure 4.11, a similar corrosion rate trend is observed at temperature of 50°C and 80°C. The corrosion rate decreases with present of Ca^{2+} in the solution and increases with increasing Ca^{2+} concentration from 7000ppm and 20000ppm. Ca^{2+} in the solution will form calcium carbonate, $CaCO_3$ scale on the metal surface and, hence, reduce the corrosion rate [26]. In addition, Ca^{2+} increases the pH value of the solution which causes the increase of Henry's constant of CO_2 in the solution, hence lower the CO_2 solubility in the solution [7]. This will cause the solution to be less corrosive, hence reduces the corrosion rate. Reduces in corrosion rate due to the present of Ca^{2+} is strongly supported from the studies conducted by Mahbob which recorded a reduction of corrosion rate from 1.225 mm/year to 0.1611mm/year due to the present of Ca^{2+} in the solution [18]. In addition, Ca^{2+} can also change the formation of corrosion scales [7]. Increase in Ca^{2+} will cause the corrosion scale become looser which cause the protectiveness of scales decrease. A high corrosion rate can be observed at high Ca^{2+} concentration because the corrosive ions will diffuse through these loose corrosion scales [7].

4.2.2 Effect of temperature

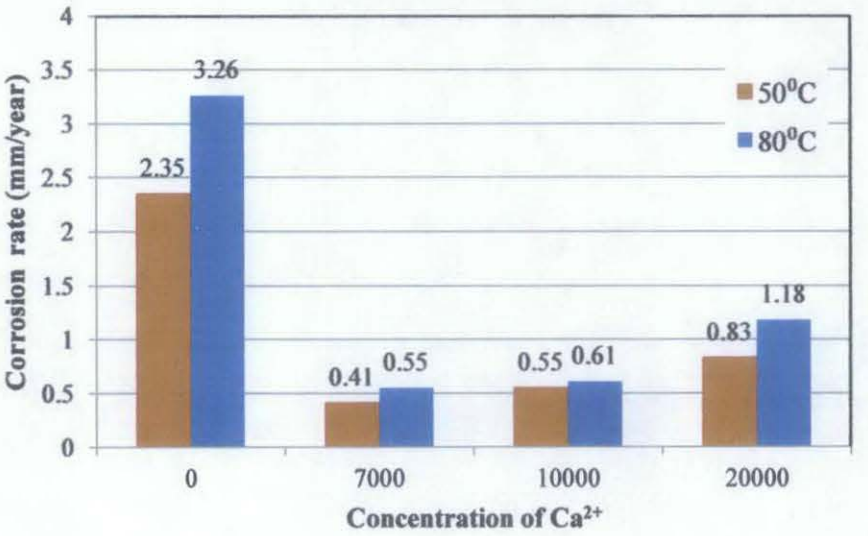

Figure 4.12: Corrosion rate at temperature of 50°C and 80°C.

A significant effect of temperature on the corrosion rate with the present of Ca^{2+} in the solution can be observed in Figure 4.12. The corrosion rate increase with increasing temperature from 50°C to 80°C. This observation can be explained base on anodic and cathodic reaction.

The effect of temperature on anodic and cathodic reactions is shown is Table 4.2. Table 4.2 shows the value of corrosion potential, E_{corr} and current density, I_{corr} after 2 hours of

exposure. The effect of temperature on corrosion rate can be explained as the following: firstly, significant increases in current density, I_{corr} indicate the acceleration of cathodic reaction with the increase of temperature from 50°C to 80°C (refer to Fig. 4.13); secondly, general trend of increasing corrosion potential, E_{corr} indicate the acceleration of anodic reaction (refer to Fig. 4.14). These two reasons lead to an increase in corrosion rate. In the agreement of Schmitt et al., the increase in temperature up to 80°C will increase the rate of chemical reaction, transport of chemical species to and from the bulk solution and the electrochemical reaction rate at the metal-solution interface [12].

Table 4.2: E_{corr} and I_{corr} at various Ca^{2+} concentrations and temperatures

Temperature (°C)	Concentration of Ca^{2+} (ppm)	E_{corr} (mV)	I_{corr} (mA/cm^2)
50	0	-689.25	0.203
	7000	-642.76	0.035
	10000	-829.81	0.047
	20000	-661.61	0.071
80	0	-688.07	0.282
	7000	-648.49	0.047
	10000	-653.43	0.052
	20000	-669.75	0.101

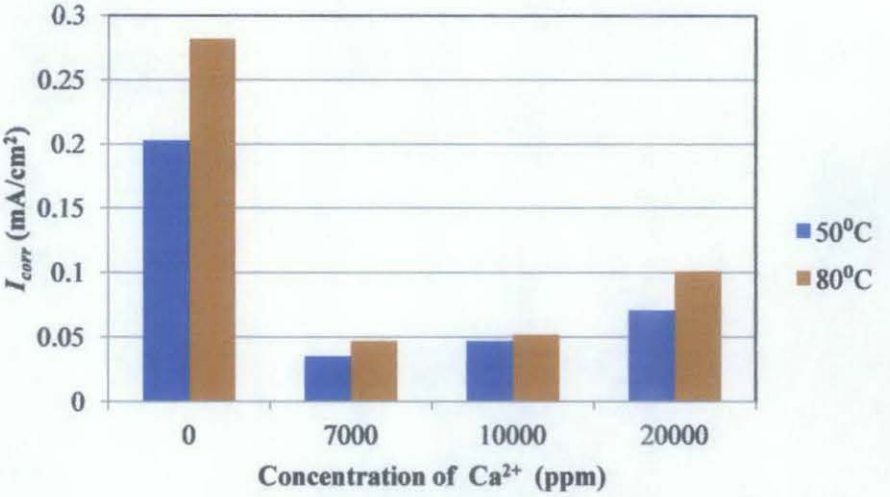

Figure 4.13: Current density, I_{corr} versus Ca^{2+} concentration

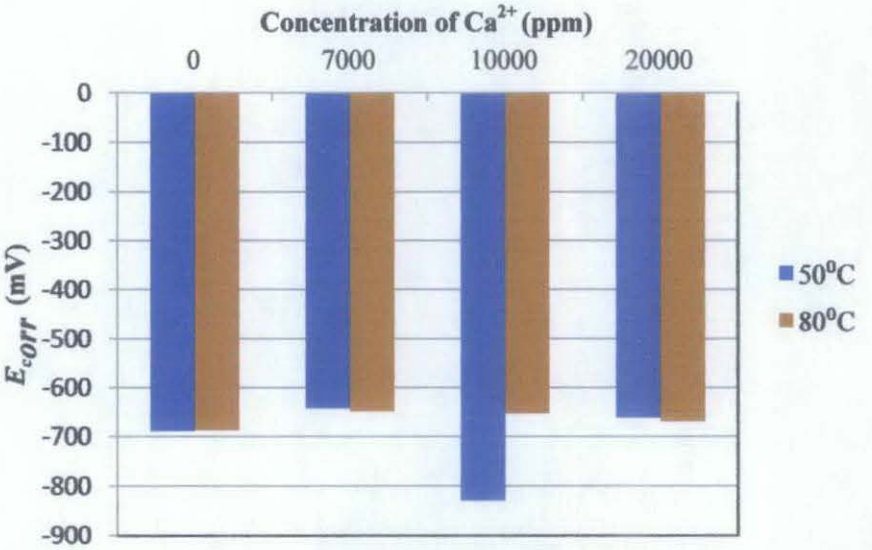

Figure 4.14: Corrosion potential, E_{corr} versus Ca^{2+} concentration

CHAPTER 5

CONCLUSION AND RECOMMENDATIONS

5.1 Conclusion

1. At the same Cl^- concentration, the corrosion rate decreases with present of Ca^{2+} in the solution and increases with increasing Ca^{2+} concentration from 7000ppm to 20000ppm.
2. In the solution containing Ca^{2+}, $CaCO_3$ scale forms a protective layer on the metal surface. However, increase in Ca^{2+} will cause the corrosion scales become looser, which will cause the protectiveness of scales decrease [7].
3. The corrosion rate increase with increasing temperature from 50°C to 80°C.
4. This is due to the acceleration of anodic and cathodic reactions when temperature increases. Increase in temperature will increase the rate of chemical reaction, transport of chemical species to and from the bulk solution and the electrochemical reaction rate at the metal-solution interface [12].

5.2 Recommendations

1. Investigate the effect of flow condition on CO_2 corrosion in the present of Ca^{2+} by using the Rotation Cylinder Electrode (RCE) to simulate the turbulence flow condition.
2. Investigate the morphology of the formation scales by using Scanning Electron Microscopy (SEM) and X-Ray Diffraction (XRD).

REFERENCES

[1] A. B. M. Merdhah, "The Study of Scale Formation in Oil Reservoir during Water Injection at High-Barium and High-Salinity Formation Water", Master of Eng. thesis, Universiti Teknologi Malaysia, 2007.

[2] A. Dugstad, E. Gulbrandesen, J. Kvarekval, R. Nyborg and M. Seiersten, " Corrosion Testing in Multiphase Flow, Challenges, and Limitation", Paper no. 6598, NACE International, Houston, Texas, 2006.

[3] A. Dugstad, "Formation of Protective Corrosion Films during CO_2 Corrosion of Carbon Steel", Eurocorr'97, Norway, Trondheim, 1997.

[4] A. Dugstad, "Fundamental Aspects of CO_2 Metal Loss Corrosion Part I: Mechanism", Paper no. 6111, NACE International, Houston, Texas, 2006.

[5] A. Muñoz, J. Genesca, R. Duran and J. Mendoza, " Mechanism of $FeCO_3$ Formation on API X70 Pipeline Steel in Brine Solutions Containing CO_2", Paper no. 297, NACE International, Houston, TX, 2005.

[6] B. R. Linter and G. T. Burstein, "Reactions of Pipeline Steels in Carbon Dioxide Solutions", 1998.

[7] Chen Ding, Ke Wei Gao and Chang Feng Chen, "Effect of Ca^{2+} on CO_2 corrosion properties of X65 pipeline steel", International Journal of Minerals, Metallurgy and Minerals, Volume 16, Number 6, December 2009, Page 661.

[8] D. G. Li, Y. R. Feng and M. S. Zheng, "Characteristics of CO_2 Corrosion Scale Formed on N80 steel in Stratum Water with Saturated CO_2". Applied Surface Science 2007, 253 (2007), 8371–8376.

[9] "Electrochemical Impedance Spectroscopy Study of the Corrosion Behavior of Some Niobium Bearing Stainless Steels in 3.5% NaCl", Retrieved on October 31, 2010 from http://www.electrochemsci.org/papers/1040171.pdf

[10] ExproBase, "CO_2 Corrosion", Retrieved on October 29, 2010 from http://www.exprobase.com/Default.aspx?page=126

[11] G. Lin, M. Zheng, Z. Bai and G. Zhao, "Effect of Temperature and Pressure on the Morphology of Carbon Dioxide Corrosion Scales". NACE International, Houston, Texas, 2006.

[12] G. Schmitt and M. Hörstemeier, "Fundamental Aspects of CO_2 Metal loss Corrosion-Part II: Influence of Different Parameters on CO_2 Corrosion Mechanisms", Paper no. 06112, NACE International, Houston, Texas, 2006.

[13] G. V. Chilingar, R. Mourhatch and G.D. Al-Qahtani, "The Fundamentals of Corrosion and Scaling for Petroleum and Environmental Engineers", Gulf Publishing Company: 2008.

[14] H. Fang, S. Nesic, and B. Brown, "General CO_2 corrosion in High Salinity Brine", Paper no. 06372, NACE International, Houston, Texas, 2006.

[15] J. C. Scully, "The Fundamentals of Corrosion", 3rd ed.; Pergamon Press: 1990.

[16] Linda G.S. Gray, Bruce G. Anderson, Michael J. Danysh, and Peter R. Tremaine,"Mechanisms of Carbon steel Corrosion in Brines Containing Dissolved Carbon Dioxide at pH 4", , Paper no. 464, NACE International, Houston, Texas, 1989.

[17] "Linear Polarization Resistance (LPR) General Information", Retrieved on October 31, 2010 from http://www.caproco.com/catalog/pdf/Probes-Instruments/Linear-Polarization-Resistance/LPR-General-Information.pdf

[18] M. I. Mahbob, "Effect of Ca^{2+} and Cl^- ions on CO_2 corrosion using electrochemical noise analysis", Bachelor of Eng. thesis, Universiti Teknologi PETRONAS, Malaysia, 2010.

[19] M. Ueda and A. Akeda, "Effect of Microstructure and Cr Content in Steel on CO_2 Corrosion", Paper no. 13, NACE International, Houston, Texas, 1996.

[20] M. Ueda and H. Takabe, "Effect of Environmental Factor and Microstructure on Morphology of Corrosion Products in CO_2 Environments", Paper no. 13, NACE International, Houston, TX, 1999.

[21] P. I. Nice, H. Takabe and M. Ueda, "The Development and Implementation of a New Alloyed Steel for Oil and Gas Production Wells", Paper no.154, NACE International, Houston, Texas, 2000.

[22] R. L. Martin, "Corrosion Consequences of Oxygen Entry into Oilfield Brines", Paper no. 270, NACE International, Houston, Texas, 2002.

[23] S. Nesic and K.J. Lee, "The Mechanistic Model of Iron Carbonate Film Growth and the Effect on CO2 Corrosion of Mild Steel", Paper no.237, NACE International, Houston, Texas, 2002.

[24] T. L. Brown, H. E. LeMay and B. E. Bursten, "Chemistry: The Central Science", 10th ed., Pearson Education Inc.: 2006.

[25] W. D. Callister, "Material Science and Engineering: An Introduction", 7th ed.; John Wiley & Sons Inc.: 2007.

[26] X. Jiang, Y.G. Zheng, D.R. Qu and W. Ke, " Effect of calcium ions on pitting corrosion and inhibition performance in CO_2 corrosion of N80 steel", Corrosion Science 48 (2006) 3091-3089.

APPENDIX 1

Linear Polarization Resistance Result

Table 1: LPR result for 0 ppm Ca^{2+} at 50°C, Ba, Bc = 120 mV and surface area = 0.64 cm^2

(Attempt#1)

Time (Sec)	LPR (ohm.cm²)	*Icorr* (mA/cm²)	Corrosion Rate (mm/year)	Potential (mV)
0	101.06	0.258122	2.9916	-694.61
362.67	156.07	0.167143	1.9371	-694.81
1033	136.58	0.190996	2.2136	-689.82
1563.2	105.94	0.246237	2.8538	-692.13
2163.6	101.85	0.256123	2.9684	-692.57
2833.4	122.73	0.212541	2.4633	-692.97
3364	118.77	0.219626	2.5454	-692.59
3964.2	129.14	0.201993	2.341	-691.85
4634.6	137.45	0.189779	2.1995	-685.39
5164.7	117.61	0.221799	2.5706	-690.49
5764.8	108.42	0.240599	2.7885	-690.9
7160.9	128.79	0.202543	2.3474	-689.25

Table 2: LPR result for 0 ppm Ca^{2+} at 80°C, Ba, Bc = 120 mV and surface area = 0.64 cm^2

(Attempt#1)

Time (Sec)	LPR (ohm.cm²)	*Icorr* (mA/cm²)	Corrosion Rate (mm/year)	Potential (mV)
0	62.053	0.420395	4.8723	-684.78
600.24	69.312	0.376367	4.362	-693.03
1200.2	78.631	0.331762	3.8451	-696.82
1800.3	69.233	0.376796	4.367	-697.6
2400.6	73.135	0.356693	4.134	-697.36
3000.8	72.888	0.357904	4.1481	-696.61
3600.9	81.414	0.320423	3.7136	-697.14
4201.3	85.107	0.306518	3.5525	-695.54
4801.4	86.774	0.30063	3.4843	-693.24
5533.3	89.669	0.290923	3.3717	-692.47
6059.6	89.254	0.292276	3.3874	-688.7
6602.1	92.63	0.281624	3.264	-688.07

Table 3: LPR result for 7000 ppm Ca^{2+} at 50°C, Ba, Bc=120 mV and surface area=0.64cm^2

(Attempt#1)

Time (Sec)	LPR (ohm.cm²)	*Icorr* (mA/cm²)	Corrosion Rate (mm/year)	Potential (mV)
0	151.69	0.1719732	1.9931	-675.52
600.32	177.78	0.146736	1.7006	-680.88
2176.8	266.53	0.0978745	1.1343	-683.05
2309.5	256.16	0.1018361	1.1802	-683.15
2909.5	310.73	0.0839525	0.9730099	-681.14
3609.7	325.51	0.0801404	0.9288269	-678.02
4186.4	388.88	0.0670815	0.7774751	-675.59
4709.9	461.29	0.0565517	0.6554343	-667.3
5310.2	654.47	0.0398591	0.461967	-654.35
5910.6	690.32	0.0377896	0.4379817	-643.66
6510.8	705.17	0.0369935	0.4287545	-641.56
7111.3	737.43	0.035375	0.4099968	-642.76

Table 4: LPR result for 7000 ppm Ca^{2+} at 80°C, Ba, Bc=120 mV and surface area=0.67cm^2

(Attempt#1)

Time (Sec)	LPR (ohm.cm²)	*Icorr* (mA/cm²)	Corrosion Rate (mm/year)	Potential (mV)
0	85.545	0.304949	3.5343	-680.56
1082.8	218.11	0.119602	1.3861	-674.4
1853	253.64	0.102848	1.192	-661.95
2753.1	290.35	0.089846	1.0413	-660.48
3653.5	448.61	0.058151	0.673965	-662.82
4554.2	397.09	0.065694	0.761395	-659.51
5453.6	410	0.063627	0.737433	-657.49
6353.7	488.83	0.053366	0.618506	-656.73

Table 5: LPR result for 7000 ppm Ca^{2+} at 80°C, Ba, Bc=120 mV and surface area=0.67cm^2 **(Attempt#2)**

Time (Sec)	LPR (ohm.cm²)	*Icorr* (mA/cm²)	Corrosion Rate (mm/year)	Potential (mV)
0	120.21	0.2170001	2.515	-693.7
600.38	249.4	0.1045969	1.2122	-674.25
1200.6	300.29	0.0868703	1.0068	-663.58
1800.7	332.48	0.0784597	0.9093482	-659.92
2400.9	368	0.0708875	0.8215866	-658.15
3001.4	409.36	0.063725	0.7385728	-655.83
3601.6	423.92	0.0615373	0.7132176	-654.63
4201.9	477.89	0.0545878	0.6326722	-652.51
4802.2	479.98	0.05435	0.6299169	-650.4
5402.7	512.03	0.0509471	0.5904771	-650.19
6003.1	514.87	0.0506669	0.5872293	-649.15
6603.5	554.59	0.0470376	0.5451661	-648.49

Table 6: LPR result for 10000 ppm Ca^{2+} at 50°C, Ba, Bc = 120mV and surface area = 0.67cm^2 **(Attempt#1)**

Time (Sec)	LPR (ohm.cm²)	*Icorr* (mA/cm²)	Corrosion Rate (mm/year)	Potential (mV)
0	168.74	0.1545961	1.7917	-814.93
600.23	364.99	0.0714713	0.8283526	-7.91E+02
1200.5	441.8	0.0590466	0.6843505	-791.16
1801	553.97	0.0470909	0.545783	-793.9
2401.2	580.67	0.0449252	0.5206836	-797.34
3001.6	598.19	0.0436095	0.5054347	-800.23
3601.7	618.59	0.042171	0.4887615	-803.27
4201.7	593.6	0.0439467	0.5093426	-805.07
4802.2	578.19	0.0451182	0.5229201	-806.75
5402.4	595.95	0.0437737	0.5073371	-808.92
6002.6	623.74	0.0418234	0.4847327	-809.59
6602.7	581.61	0.0448527	0.5198432	-809.79

Table 7: LPR result for 10000 ppm Ca^{2+} at 50°C, Ba, Bc = 120mV and surface area = 0.67cm^2 **(Attempt#2)**

Time (Sec)	LPR (ohm.cm²)	*Icorr* (mA/cm²)	Corrosion Rate (mm/year)	Potential (mV)
0	185.62	0.140533	1.6287	-849.62
600.18	302.9	0.0861239	0.9981756	-837.78
1200.5	367.54	0.0709761	0.8226128	-840.05
1800.9	455.45	0.0572772	0.6638432	-839.09
2401.2	455.44	0.0572782	0.6638544	-837.15
3072.6	370.86	0.07034	0.8152408	-838.96
3716.1	401.58	0.0649607	0.7528948	-842.24
4316.7	439.64	0.059336	0.6877038	-840.65
4917.1	518.4	0.050322	0.5832315	-838.9
5517.8	555.14	0.0469914	0.5446303	-836.57
6002.3	545.83	0.0477931	0.5539216	-832.06
6602.6	550.47	0.0473902	0.549253	-829.81

Table 8: LPR result for 10000 ppm Ca^{2+} at 80°C, Ba, Bc = 120mV and surface area = 0.67cm^2 **(Attempt#1)**

Time (Sec)	LPR (ohm.cm²)	*Icorr* (mA/cm²)	Corrosion Rate (mm/year)	Potential (mV)
0	92.653	0.2815536	3.2632	-691.29
600.42	197.67	0.1319679	1.5295	-687.41
1200.7	262.2	0.0994921	1.1531	-679.72
1801	319.54	0.0816369	0.9461718	-671.98
2401.3	371.23	0.0702711	0.8144416	-665.89
3001.5	392.71	0.0664273	0.7698928	-661.83
3601.6	412.92	0.0631757	0.7322061	-658.71
4201.9	430.28	0.0606278	0.702676	-657.4
4802.4	446.11	0.0584758	0.6777346	-655.84
5402.9	477.29	0.0546554	0.6334561	-654.67
6002.9	482	0.0541221	0.6272755	-653.62
6603	497.45	0.0524413	0.6077944	-653.43

Table 9: LPR result for 20000 ppm Ca^{2+} at 50°C, Ba, Bc = 120mV and surface area = 0.64cm^2 **(Attempt#1)**

Time (Sec)	LPR (ohm.cm²)	*Icorr* (mA/cm²)	Corrosion Rate (mm/year)	Potential (mV)
0	82.802	0.3150494	3.6514	-694.19
658.4	98.845	0.2639175	3.0588	-693.12
1190.7	108.42	0.2405949	2.7884	-691.83
1856	124.83	0.2089665	2.4219	-687.13
2387.7	149.92	0.1739949	2.0166	-683.97
3272.1	198.5	0.1314181	1.5231	-676.58
3670.5	211.48	0.1233491	1.4296	-670.68
4203.1	250.08	0.1043108	1.2089	-667.31
4734.8	289.84	0.090002	1.0431	-664.86
5236.5	306.99	0.0849751	0.9848608	-662.43
5836.7	328.37	0.0794436	0.9207514	-662.29
6854.4	365.63	0.0713466	0.8269069	-661.61

Table 10: LPR result for 20000 ppm Ca^{2+} at 80°C, Ba, Bc = 120mV and surface area = 0.64cm^2 **(Attempt#1)**

Time (Sec)	LPR (ohm.cm²)	*Icorr* (mA/cm²)	Corrosion Rate (mm/year)	Potential (mV)
0	74.76	0.34894	4.0442	-696.16
599.95	96.417	0.270563	3.1358	-696.15
1307.1	110.75	0.235547	2.7299	-695.4
1800.2	117.24	0.222508	2.5788	-694.57
2400.2	141.12	0.184852	2.1424	-693.87
3109.3	165.29	0.157822	1.8291	-689.5
3600.3	179.77	0.145113	1.6818	-690.13
4200.5	202.3	0.128947	1.4944	-688.31
4911.3	209.54	0.124492	1.4428	-685.76
7111.1	281.63	0.092627	1.0735	-679.09
7244	279.11	0.093464	1.0832	-677.74
7844.2	314.28	0.083003	0.96201	-675.89

Table 11: LPR result for 20000 ppm Ca^{2+} at 80°C, Ba, Bc =120mV and surface area= 0.64cm^2**(Attempt#2)**

Time (Sec)	LPR (ohm.cm^2)	*Icorr* (mA/cm^2)	Corrosion Rate (mm/year)	Potential (mV)
0	92.752	0.2812535	3.2597	-682.88
573.39	98.754	0.26416	3.0616	-6.82E+02
1127.4	121.07	0.2154642	2.4972	-681.46
1680.8	138.58	0.1882349	2.1816	-680.29
2404.1	189.46	0.1376892	1.5958	-678.5
3045.6	194.97	0.1337955	1.5506	-676.85
3711.3	191.14	0.136478	1.5817	-675.35
4109.9	228.14	0.1143439	1.3252	-674.31
4726.3	212.77	0.1226028	1.4209	-673.98
5282.5	255.86	0.1019545	1.1816	-672.07
5969.5	257.5	0.1013047	1.1741	-671.31
6482.8	257.08	0.1014724	1.176	-669.75